Non-sequential injection of PGE-rich ultramafic sills in the Platreef Unit at Akanani, Northern Limb of the Bushveld Complex: Evidence from Sr and Nd isotopic systematics

Roger Scoon, Gelu Costin, Andrew Mitchell, Bertrand N. Moine

Non-sequential injection of PGE-rich ultramafic sills in the Platreef Unit at Akanani,

Northern Limb of the Bushveld Complex: Evidence from Sr and Nd isotopic systematics

Roger N Scoon
Department of Geology, Rhodes University, Grahamstown, South Africa
e-mail: rnscoon@iafrica.com

Gelu Costin
Department of Earth, Environmental and Planetary Sciences, Rice University, Houston, TX, 77005, USA
e-mail: g.costin@rice.edu

Andrew Mitchell
PO Box 421, McGregor 6708, South Africa
e-mail: mitchaa@mweb.co.za

And

Bertrand Moine
Université de Lyon, UJM-Saint-Etienne, Laboratoire Magmas et Volcans, UJM-UCA-CNRS-IRD, 23 rue Dr. Paul Michelon, 42023 Saint Etienne, France e-mail: bertrand.moine@univ-st-etienne.fr

Abstract

The Platreef Unit is a deceptively complex sequence of layered cumulates located in the northern limb of the 2.055 Ga-old Bushveld Complex. The unit includes the Platreef, a thick, richly mineralized stratabound PGE orebody which differs markedly from the comparatively thin, predominantly stratiform Merensky Reef found in the Upper Critical Zone of the eastern and western limbs. The Platreef Unit is, however, interpreted as a localized facies of the Upper Critical Zone, despite layering being neither as systematic nor as clearly defined as in the equivalent stratigraphy found in the other limbs. The Platreef Unit in the Akanani project area includes well-defined layers of feldspathic harzburgite and norite, in addition to the ubiquitous feldspathic orthopyroxenite-melanorite that characterizes other sections. The paucity of floor-rock xenoliths is an additional feature. The relatively well-developed nature of the layering and paucity of xenoliths in the Platreef Unit at Akanani is explained by separation of the unit from the floor of the intrusion by a thick succession of ultramafics assigned to the Lower Critical Zone. We identify three lithological subgroups in the Platreef Unit at Akanani. They do not define an upward-younging stratigraphy. The primary stratigraphy, or PU1 subunit, is dominated by multiple layers of feldspathic orthopyroxenite, melanorite, and norite. This subunit built up from incremental addition of relatively small magma pulses. Repeated magma replenishment induced concomitant partial melting of earlier-formed layers. The PU1 subunit includes thin chromite stringers that contain Cr-spinels with unusual, amoeboidal textures consistent with several stages of growth and re-equilibration. The feldspathic harzburgite of the younger PU2 subunit was emplaced non-sequentially into the already complexly-layered PU1 subunit as a series of sinuous lenses or syn-intrusive sills. One of the PU2 sills contains the richest and most consistent of the mineralized sections at Akanani, i.e., the Main Mineralized Reef

(MMR). The irregularly-developed pegmatoidal lithologies of the PU3 subunit are ascribed to recrystallization of earlier-formed cumulates (PU1 and PU2).

Whole rock isotopic data for a section of the Platreef Unit, together with the overlying Lower Main Zone and underlying Lower Critical Zone, mostly from drill-hole ZF-1, demonstrate a complex pattern in both Sr_{87}/Sr_{86} initial ratios and ε_{Nd} values. These patterns are consistent with multiple lineages of parental magmas. The Lower Main Zone and the majority of the Platreef Unit are characterized by anomalously high Sr initial ratios (with a large degree of scatter) and low ε_{Nd} values (relatively tightly constrained). Harzburgite layers from the Lower Critical Zone have a low Sr initial ratio and a relatively high ε_{Nd} value. The new isotopic data suggest these sequences crystallized from multiple magma batches, broadly constrained within the U-type (ultramafic) and A-type (tholeiitic) lineages, derived from mantle sources and/or staging chambers which experienced varying degrees of crustal contamination. The MMR crystallized from a specific pulse of the U-type magma lineage characterized by a high Sr_{87}/Sr_{86} initial ratio (average of 0.71113) and a markedly low ε_{Nd} value (average of -11.35). The olivine-saturated magmas associated with the MMR were derived from a localized mantle source and yet underwent an unusually high degree of crustal contamination. Some of layered PGE orebodies in the Bushveld Complex, including the Platreef and Merensky Reef, were emplaced as syn-magmatic sills which crystallized from anomalously PGE-rich parental magmas with an unique isotopic fingerprint.

Keywords:

Bushveld Complex; PGE-rich Magma; Platreef; Syn-intrusive sills; Sr and Nd Isotopes

Introduction

The Platreef Unit is part of the Rustenburg Layered Suite, the most intensively studied component of the Bushveld Igneous Complex, South Africa. This unit contains an unusually thick and richly mineralized stratabound PGE orebody i.e., the Platreef. The Platreef is restricted to the northern limb of the complex, and was recognized at an early stage as representing the lateral equivalent of the thin, predominantly stratiform Merensky Reef of the eastern and western Limbs (Wagner, 1929). More recent investigations interpret the Platreef as comparable with the entire Upper Critical Zone (e.g., Viljoen & Schürmann, 1998; McDonald & Holwell, 2011; Viljoen, 2016). We recommend usage of the term Platreef Unit, as proposed by Mitchell & Scoon (2012), rather than simply Platreef, in order to facilitate the discussion of the weakly mineralized or barren lithologies associated with the richly mineralized components as part of the same overall phenomenon.

The Akanani project area is located several hundred kilometres north of Pretoria, near the regional centre of Mokopane (Fig. 1). The resource occurs at depth, and is known only from an extensive drilling program (Mitchell, 2006). The sequence that hosts the mineralization at Akanani is relatively thick and multiple mineralized intervals are recognized (Yudovskaya et al., 2011; Mitchell & Scoon, 2012; Van der Merwe et al., 2012). Akanani is located on the western boundary of several large open pit deposits, and a view of the plateau in this area shows the paucity of outcrop (Fig. 2a). The open pit resources have been described in great detail (e.g., Armitage et al., 2001; Hutchinson & Kinnaird, 2005; Kinnaird et al., 2005; McDonald et al., 2005; Sharman-Harris et al., 2005; Holwell & Jordaan, 2006; Holwell et al., 2007), but there are several advantages of studying the Platreef Unit at Akanani. First, the succession is more prominently layered than in the open pits and includes feldspathic

harzburgite and norite in addition to the ubiquitous feldspathic orthopyroxenite-melanorite. Second, the Platreef Unit at Akanani is separated from the floor of the intrusion by a thick sequence of ultramafics which are equated with the Lower Critical Zone. Floor-rock xenoliths which severely affect the near-surface resources (Fig. 2b), as described by, for example, Buchanan et al. (1981) and Harris and Chaumba (2001), are almost entirely absent from the Platreef Unit at Akanani.

The samples for the new study are mostly from drill-hole ZF-1, located in the southeastern part of the Akanani project area (Fig. 3). Detailed logging of this drill-hole has confirmed the deceptively complex nature of the layering within the Platreef Unit. Petrographic descriptions and electron microprobe analyses are presented for some of the ultramafic layers. Cr-spinels with unusual, amoeboidal textures are described from thin chromite stringers. New whole-rock Sr and Nd isotopic data are presented for the Platreef Unit, together with parts of the overlying (Lower Main Zone) and underlying (Lower Critical Zone) stratigraphy. These data are compared with published isotopic data for the Lower Main Zone and Platreef Unit from the Sandsloot and Overysel sections.

Syn-magmatic Sills

The layering of the Platreef Unit at Akanani is far more complex than is generally recognized and is unlikely to represent a simplistic, upward-younging layercake stratigraphy. Individual layers cannot necessarily be correlated between the drill-cores at Akanani and some layers are clearly discordant (Mitchell, 2006). We revisit the hypothesis of Mitchell & Scoon (2012) that some ultramafic magma sheets at Akanani were injected as syn-magmatic sills into a pre-existing, subsolidus cumulate sequence. This hypothesis is consistent with

the possibility that the majority of ultramafic layers that are intercalated with noritic-anorthositic cumulates in the RLS, including the Merensky Reef, may have a similar origin (Mitchell, 1996; Mitchell & Scoon, 2007; Voordouw et al., 2009; Mungall et al., 2016; Scoon and Costin, 2018; Mitchell et al., 2019a). The hypothesis of syn-magmatic sills to explain some of the complexities of the Upper Critical Zone layering in the eastern and western limbs of the intrusion has, however, caused some debate (e.g., Latypov et al., 2017), but this has arisen in part due to a number of misconceptions and over-simplifications, as discussed by Scoon and Mitchell (2018). The hypothesis of syn-magmatic sills is consistent with the field knowledge and has an important bearing on the current study. Comparisons between some of the PGE mineralized intervals of the northern limb and the eastern/western limbs are justified, and we do not subscribe to an approach whereby the Platreef Unit is treated as an entirely separate phenomenon.

Regional Geology

The oldest component of the Bushveld Igneous Complex i.e., the Rooiberg Group, was a giant extrusive event that flooded the centre of the Transvaal Basin with sheets of rhyolite (felsite) and granophyre up to 6 km thick (Walraven et al., 1990). The Rustenburg Layered Suite (RLS) was primarily intruded beneath the Rooiberg felsites and granophyres into the uppermost part of the Transvaal Supergroup, i.e., the Pretoria Group (Hall, 1932). In part of the northern limb, the RLS cuts into the cratonic basement (Fig. 1). The RLS is overlain (and partly intruded) by thick sheets of granite and granophyre, collectively known as the Lebowa Granite Suite. The granitic sheets have displaced the older felsites as the roof to the RLS throughout the northern limb.

Geochronology

The Rooiberg Group has been dated at 2.061 Ga (Cawthorn & Walraven 1998) and the RLS at 2.055 Ga (Scoates & Friedman, 2008). The precise U-Pb geochronology of Mungall et al. (2016) indicates that the RLS formed over a period of at least 0.6 Ma (2056.28±0.15-2055.54±27 Ma). The principal component of the Lebowa Granite Suite, the Nebo Granite, has an age of 2.054 Ga (Walraven & Hattingh, 1993). All three components of the Bushveld Igneous Complex may have formed in a relatively short interval, possibly due to a mantle plume (Hatton & Schweitzer, 1995; Cawthorn & Walraven 1998; Zeh et al., 2015).

The Rustenburg Layered Suite at Akanani

Subdivision of the RLS into well-defined zones (Fig. 4a), i.e. from the base upwards Marginal (MaZ), Lower (LZ), Lower Critical (LCZ), Upper Critical (UCZ), Lower Main (LMZ), Upper Main and Upper, is based on the original work of Hall (1932), Wager & Brown (1968), and Von Gruenewaldt et al. (1985), and as recommended by the South African Committee for Stratigraphy (SACS) (1990). The boundaries shown here are based on the conventional approach which to a large extent is that also recommended by SACS. A characteristic feature of the northern limb is the drastically thinned nature of the RLS (e.g., Viljoen & Schürmann, 1998).

The MaZ has not been identified in the vicinity of Akanani, but a thick, sill-like body of ultramafics located to the east of the RLS may be correlated with the LZ (Fig. 3). This interpretation is consistent with the highly irregular (and discordant nature) of the basal contact of the RLS (Fig. 4a). The individual sill- and stock-like bodies of ultramafics located east of the northern limb may connect with the RLS at depth (Fig. 4b). The most well-

known of these occurrences is the Uitloop stock, located between Akanani and Mokopane (Van der Merve, 1976; Clarke et al., 2009). We have logged and sampled a 500 m-deep drill-hole from Uitloop comprised entirely of serpentinized dunite. The presence of thick layers of dunite in the LZ of the eastern and western limbs is well known (e.g., Cameron, 1980; Teigler & Eales, 1996), but the occurrence of stock-like bodies comprised only of dunite is unusual. Moreover, a connection between the disjointed occurrences of LZ at depth is consistent with the findings of Yudovskaya et al. (2013) who described a thick tongue of LZ (that was not previously known) within the floor rocks at Sandsloot.

The occurrence of the LCZ at Akanani, as discussed by Mitchell & Scoon (2012), and shown in a cross-section (Fig. 4b), was possibly the first mention of this subzone in the northern limb. A longitudinal section presented by Viljoen (2016) shows the LCZ as a regional feature underlying the PU in the entire southern part of the Northern Limb. To the east of the Akanani project area, the Platreef Unit (PU) rests on either dolomite of the Transvaal Supergoup (in the southern part) or Archaean granite-gneiss (northern part) (Fig. 3). The thickened nature of the PU at Akanani is consistent with its location a substantial distance down-dip from the floor (Fig. 4b).

To the south of the Akanani project area, a deep resource of Platreef occurs at the Turfspruit locality. Turfspruit reveals a thick section of the PU and also includes both ultramafic and noritic layers (Yudovskaya et al., 2017a; Grobler et al., 2019). However, Turfspruit and Akanani occur in separate subchambers and there may be considerable stratigraphic differences between the two sections (we have commented on the early compartmentalization of the RLS previously: Scoon & Teigler, 1994).

The PU throughout the Northern Limb is overlain by the LMZ, of which the lowermost few hundred metres at Akanani is comprised of medium to coarse-grained norite with distinctive layers of coarse-grained mottled (oikocrystic) anorthosite, some of which are sufficiently resistant as to form outcrop (Van der Merve, 1976; Mitchell & Scoon, 2012). This is a general feature of the LMZ throughout the RLS (Mitchell, 1990; South African Committee for Stratigraphy, 1990). The PU and LMZ are generally interpreted as being in stratigraphic succession, as discussed by Holwell et al. (2005), but there is a possibility of the PU having intruded beneath and partly into the LMZ. This suggestion was made on the basis of regional mapping (Van der Merwe, 1976) and is consistent with observations that in the northern part of Akanani, as well as on the adjacent property of Drenthe (Gain & Mostert, 1982), parts of the PU may be intercalated within the LMZ (Mitchell & Scoon, 2012).

Stratigraphy of ZF-1

A detailed stratigraphic log for part of drill-hole ZF-1 illustrates the subdivision into three zones i.e., LMZ, PU, and LCZ (Fig. 5). The basal part of the LMZ in the section described here is comprised of homogenous norite with little discernible layering. The contact between the LMZ and the distinctly more mafic PU occurs at a depth of 1013.71 m (Fig. 6). The PU consists of ultramafic and noritic lithologies. We follow our earlier contribution in recognizing three subunits: PU1, PU2, and PU3; this methodology is fundamental to our study as subunits do not define an upward-younging succession (Mitchell & Scoon, 2012). The long-held tendency to describe the Platreef by a simplified stratigraphy divided into a series of units, labelled from the bottom up as A-B-C (White, 1994; Viljoen & Schurmann, 1998; Viljoen, 2016) is, therefore, misleading. The layering is far more complex than has

been previously reported and individual layers cannot necessarily be correlated between drill-cores.

The base of the PU in ZF-1 is positioned at a depth of 1110 m, although the contact with the LCZ is both gradational and subjective. The PU1 subunit is dominated by intercalated sequences of feldspathic orthopyroxenite and melanorite (Fig. 5). The modal proportion of orthopyroxene and plagioclase is variable. Clinopyroxene is relatively abundant in both lithologies, but possibly more so in the melanorite. This subunit also includes a well-defined layer of norite. Some of the ultramafic layers in the PU1 contain accessory olivine and may also contain >10 modal percent disseminated chromite. Several thin chromite stringers occur within this subunit. The PU2 subunit is comprised of well-defined layers of poikilitic feldspathic harzburgite and orthopyroxenite (± olivine). From earlier studies, we found that the PU2 subunit layers are discordant and do not occur at the same stratigraphic height in cores from neighbouring drill-holes. We reserve the PU3 subunit for coarse-grained, pegmatoidal assemblages as they are rather irregularly developed, even patchy, and only constitute well-defined layers in a handful of examples. The composition of the "pegmatoids" varies considerably and can include orthopyroxenite (± olivine), feldspathic orthopyroxenite, melanorite, and norite.

The lack of evidence for fractional crystallization cycles in the Akanani sequence was commented on by Mitchell & Scoon (2012). The upper part of the PU sequence in ZF-1 (depth of 1014-1022 m) is comprised of poorly-defined layers of coarse-grained melanorite and medium-grained feldspathic orthopyroxenite (PU1). Well-defined layers of poikilitic feldspathic harzburgite and orthopyroxenite occur at a depth of 1022-1027 m (PU2). This

component of the sequence includes pegmatoidal lithologies (PU3). Intercalated layers of melanorite and feldspathic orthopyroxenite (PU1) at a depth of 1027-1065 m are broadly similar to the sequence in the uppermost part of the unit. The thick layer of norite (PU1) intersected at a depth of approximately 1065 m reveals prominent inch-scale layering in the basal part. The norite is underlain at a depth of 1089-1094 m by a second group of ultramafic layers (PU2), some with pegmatoidal textures (PU3). The basal part of the PU at a depth of 1094-1110 m is comprised of a complex sequence of feldspathic orthopyroxenite (PU1) and olivine-bearing orthopyroxenite (PU2). Cr-spinel is notably abundant in the upper part of this interval.

The layers of poikilitic feldspathic harzburgite assigned to the PU2 subunit are very similar to the well known Tarantaal marker in the Pseudo Reef Unit of the Swartklip facies, Western Limb (Mitchell & Scoon, 2012). The diagnostic speckled texture arises from the presence of interstitial plagioclase (15-20 modal %) together with large oikocrysts of orthopyroxene within a matrix of olivine (Viljoen et al., 1986; Mitchell et al., 2019b). The harzburgite at Akanani is partially serpentinized (Fig. 7a) which has caused some confusion with xenolithic material. The patchy development of the pegmatoidal texture in some of the layers of orthopyroxenite is emphasized (Fig. 7b). The thin chromite stringers located at a depth of approximately 1097 m occur parallel to the primary layering (Fig. 7c). The harzburgite from the LCZ is notably less felsic in comparison to that from the PU2 (Fig. 7d).

Mineralization in ZF-1

The PU1 subunit is typically weakly mineralized, and the richer grades in ZF-1 (and other drill-cores at Akanani) are associated with the PU2 and PU3 subunits (Fig. 8). The

relationship between PGE and well-defined layers of poikilitic feldspathic harzburgite at Akanani was highlighted by Mitchell & Scoon (2012). Multiple ore-layers are definable, but the principal mineable reserve, constrained by both grade and lateral continuity, is the Main Mineralized Reef (MMR). The MMR is associated with the stratigraphically highest occurrence of the PU2 subunit in all of the drill-holes described by Mitchell & Scoon (2012), including ZF-1. The thickness of the MMR is variable, in part as it may incorporate some of the adjacent PU1 subunit. The pattern of mineralization in ZF-1 is rather unusual as the MMR is not particularly well developed and richer peaks (described here as Lower Reefs) are identified.

Sampling

Quarter sections of drill-core were obtained from two drill-holes, ZF-1 and MO-3 (Fig. 3). Samples are referenced relative to depth (Table 1). The main batch of samples submitted for isotopic analysis is from ZF-1 (25 samples). The ZF-1 samples are divided into the following stratigraphic groups LMZ (5 samples), PU (17 samples), and LCZ (3 samples). Samples are constrained to identifiable uniform layers (Fig. 5) with the exception of ZF-1/1085.8 (inch-scale layered pyroxenite-norite), and ZF-1/1096.8 and ZF-1/1097.2 (chromite stringers). Four samples were analysed from MO-3.

Analytical Methods

Polished thin sections were prepared from selected samples, with EPMA data acquisition performed at Rhodes University on a Jeol JXA 8230 Superprobe using 4 WD spectrometers. Analytical conditions employed for quantitative analysis of mafic silicates (olivine, clinopyroxene) were: 15 kV acceleration voltage, 20 nA beam current, and spot beam size

(ca. 1 micron). The counting time per peak was 20 sec for each element (10 sec for peak and 5 sec for each lower and upper background, respectively), with the exception of Ni, where a 45 sec counting time was preferred (30 sec per peak and 15 sec per each upper and lower background, respectively). The standards used for calibration were natural minerals, as follows: pentlandite for Ni (Kα), olivine (Fo_{93}) for Si (Kα), Mg (Kα) and Fe (Kα), plagioclase for Al (Kα), diopside for Ca (Kα), rhodonite for Mn (Kα), rutile for Ti (Kα), chromite for Cr (Kα), jadeite for Na (Kα), and biotite for K (Kα). The following analytical conditions were employed for plagioclase: 15 kV accelerating voltage, 20 nA beam current, 20 microns beam size. The following standards were used: Jadeite for Na, plagioclase (An_{67}) for Si, Al and Ca, and olivine (Fo_{93}) for Mg and Fe. PRZ matrix correction was used for quantification. For chromite analysis, a chromite standard was used for calibrating the Kα lines of Fe, Cr, Mg and Al. The ZAF matrix correction method was employed for quantification of silicates, and oxides. Large and sensitive analyzing crystals (LPET and LLiF) were used to analyze elements in a low concentration such as Cr, Mn and Ni in silicates and oxides.

Rock powders were prepared in the laboratory at Rhodes University and submitted to the Laboratoire Magmas et Volcanoes, St-Etienne for trace element data and bulk rock Sm-Nd and Sr-Rb isotopic analysis. Traces were analyzed by inductively coupled plasma mass-spectrometry (ICPMS) on an AGILENT 7500 instrument. Rock powders (100 mg) were dissolved in an HF: HNO_3: $HClO_4$ mixture solution. Dried samples were taken up in HNO_3 and diluted in 2% HNO_3 of 1:4000 shortly before analysis together with blanks. Two mafic international standards (BIR1, BCR2) were used as calibration external standards and dunite JP1 used as an unknown for accuracy. For the isotopic Sr and Nd separation, samples were processed through four columns following the method of Pin et al. (1994) and Pin and

Zalduegui (1997). After evaporation and dissolution in HNO_3 2M, a coupled passage on Sr spectrometry and TRU spectrometry columns was used to separate Sr and rare earth elements. Lastly, Nd was isolated with LN spectrometry columns. Strontium isotopic measurements were performed by TIMS (TRITON) at Laboratoire Magmas et Volcans, Clermont-Ferrand, and $^{87}Sr/^{86}Sr$ ratios were normalized to $^{86}Sr/^{88}Sr$ equal to 0.1194. Neodymium isotopic and Sm-Nd concentrations were performed by isotope dilution using a mixed ^{149}Sm-^{150}Nd tracer and a MC-ICP-MS (Neptune plus coupled to an Aridus II system) also at the Laboratoire Magmas et Volcans, Clermont-Ferrand. Sr and Nd isotopic ratios are calculated based on $^{87}Sr/^{86}Sr$=0.710230±11 for NBS SRM987 and $^{143}Nd/^{144}Nd$=0.512115±16 for JNdi-1. Total procedural blanks were <1 ng for both Sr and Nd.

Petrography

The medium-to coarse-grained feldspathic orthopyroxenite, the dominant lithology of the PU1 subunit, is comprised of large grains of orthopyroxene together with interstitial clinopyroxene and plagioclase (Fig. 9a). Closely-packed grains of orthopyroxene reveal triple boundaries due to annealing (Fig. 9b). Large oikocrystic grains of orthopyroxene and small grains of amphibole may enclose earlier-formed Cr-spinel (Fig. 9c). The chromite stringers illustrated in Fig. 7 are comprised of small, rounded grains of Cr-spinel, together with interstitial orthopyroxene and flecks of biotite (Fig. 9d). Large oikocrysts of orthopyroxene in the pegmatoidal feldspathic orthopyroxenite juxtaposed with the chromite stringers enclose an earlier generation of orthopyroxene (Fig. 9e). Some of the orthopyroxene oikocrysts reveal clinopyroxene exsolution (Fig. 9f). This exsolution is not the classic geometric type, but is patchy and appears to cluster in the oikocrysts proximal to the grains of Cr-spinel.

The chromite stringers may include unusual amoeboidal grains in addition to rounder grains of Cr-spinel. Some of the amoeboidal grains contain prominent silicate cores (Figs. 10a-b). Similar features have been described by Yudovskaya et al. (2019) from the Turfspruit locality. Euhedral grains of Cr-spinel may contain silicate inclusions (Figs. 10c-d). Silicate inclusions are probably melt inclusions and preliminary analytical data (not presented here) demonstrates a broad range of compositions. The presence of apparently coalesced grains of Cr-spinel with silicate inclusions is also observed (Figs. 11a-d). The harzburgite from the LCZ is distinguished from the feldspathic harzburgite of the PU by the absence of plagioclase and presence of large oikocrysts of orthopyroxene (Fig. 12a). The olivine in the harzburgite from the LCZ is quite severely serpentinized (Fig. 12b).

Mineral Chemistry

Mineral chemistry in part supplements the data of Mitchell & Scoon (2012) and assist with discrimination of lithologies from the PU and the LCZ (see also Supplementary Data). To recap, the latter authors reported the composition of the olivine in the poikilitic feldspathic harzburgite of the MMR as having a composition of $Fo_{81.2-80.4}$ and NiO content of 0.36-0.39%. Yudovskaya et al. (2013) reported the presence of up to 0.5 wt% NiO in olivine from the feldspathic harzburgite (MMR) at Akanani. These data may be compared with the anomalously Ni-rich nature of olivine from the potholed Merensky Reef at Union Section, western limb (Scoon & De Klerk, 1987). The presence of Ni-rich olivine confirms the magmatic origin of the MMR feldspathic harzburgite (i.e. the olivine is not xenolithic: Mitchell & Scoon, 2012). Moreover, the composition of the olivine in the MMR is comparable with olivine from both the Pseudo Reef harzburgite and Merensky Reef of the Amandelbult and Union Sections, western limb (Scoon & De Klerk, 1987; Mitchell et al.,

2019b). In comparison, the olivine from the LCZ at Akanani (Fo_{88}; NiO=0.33-0.39%; sample ZF-1/1111.2) is distinctly more magnesian and can be compared with data of Teigler & Eales (1996) for the LCZ, western limb.

The orthopyroxene from the PU yields an X_{Mg} ratio of 0.83-0.89 (samples ZF-1/1096.8 and ZF-1/1097.2) and the orthopyroxene from the LCZ an X_{Mg} ratio of 0.95 (sample ZF-1/1111.2). The plagioclase in sample ZF-1/1097.2 has a broad compositional range ($An_{58.0-64.6}$) which is typical of the UCZ (e.g., Eales et al., 1986). The Cr-spinel in the chromite stringers (sample ZF-1/1097.2) has relatively low concentrations of chromium (Cr_2O_3 = 41.39-43.43%), typical of occurrences in the uppermost part of the UCZ (Eales & Reynolds, 1986). The 40-cm wide chromitite layer from the LCZ, which was analysed by Mitchell & Scoon (2012a), has a composition typical of the Lower Group chromitites (average Cr_2O_3 = 49.98%).

Whole-rock Geochemistry

Selected whole-rock trace element data are presented in Table 2. The range in Sr contents reflects the broad range in the modal proportion of plagioclase (albeit minor amounts of Sr occur in the pyroxene). The norite from the LMZ reports an average Sr content of 189.2±26.3 ppm. Mafic lithologies from the PU1 subunit (feldspathic orthopyroxenite-melanorite) report average Sr contents of 81.5±24.7 ppm (this excludes the norite from this subunit). The average Sr content of the samples from the PU2 subunit is 39.0±14.3 ppm. The low concentration of Sr (10.3±1.6 ppm) in the harzburgite from the LCZ confirms the paucity of Sr at this height. The generally positive trend between the concentrations of Sr and Y (Fig. 13a) is consistent with the broad stratigraphy i.e. LCZ (relatively primitive) through PU (intermediate) to LMZ (relatively evolved). The scatter in samples from the PU

is in part due to the modal variations noted above. The distinctly higher concentrations of Y in the PU3 subunit (despite some samples having an ultramafic composition) are significant as they may indicate a higher proportion of trapped melt. The high degree of scatter on the plot of Sr vs. Rb is largely a function of modal variations and the proportion of trapped melt (Fig. 13b).

Plots based on Zr, widely recognized as a highly incompatible element in most rock-forming silicates, can be tentatively used as an indicator of the proportion of trapped melt (Fig. 14). The plot of Zr vs. Nb is consistent with the generalized fractional crystallization trend noted above: samples from the LCZ are the least fractionated, the PU reveals a range in fractionation, and the norite from the LMZ is the most fractionated. Most of the other plots, including Zr vs. V, Zr vs. Y and Zr vs. Sr reveal degrees of scatter due to combinations of modal effects and varying proportions of trapped melt. The scatter on the plots of Zr vs. Ni and Cu is related to the presence of relatively small amounts of base-metal sulphides. Plots of Zr vs. Sm and Zr vs. Nd reveal broad correlations with some degree of scatter (Fig. 15a, b). The plot of Sm vs. Nd shows a good correlation. The LCZ and LMZ are clearly discriminated, as is the intermediate position of the PU (Fig. 15c). An interesting observation apparent both here, and on the plots of Zr vs. Sm and Zr vs. Nd, is the relatively primitive nature of the PU2 samples relative to the PU1 (they represent a reversal).

Sr Isotopic Systematics

The new whole rock Sr isotopic data are presented in Table 3 (initial ratios were normalized to an age of 2.055 Ga). Averages for the new data are compared with averages of some published data in Table 4. The five samples of the LMZ from drill-hole ZF-1 have a relatively

tightly constrained Sr-initial ratio (average of 0.70892). The samples from the PU (excluding PU2) report a slightly higher Sr-initial ratio (average of 0.70972), but with a noticeably poorer standard deviation. A degree of scatter is evident when these data are plotted against the vertical log (Fig. 16). This scatter is thought to be a primary feature, not due to localized contamination (noting the absence of xenolithic material). The samples from the MMR report a distinctly higher Sr-initial ratio (average of 0.71113). The LCZ reveals a range of Sr-initial ratios, albeit the two samples of the harzburgite are tightly constrained. The anomalous Rb/Sr ratio of sample ZF-1/1111.2 possibly reflects the paucity of Sr in this sample. A plot of the Sr initial ratio vs. Zr shows a high degree of scatter with little evidence of modally-controlled variations (Fig. 15d). The four samples from drill-hole MO-3 (LMZ and PU) yield similar initial ratios to data from ZF-1.

In comparing the new data with published analyses we have had some difficulties due to problems with stratigraphic correlations. Averages for some of the published data presented in Table 4 are based on our assumptions of the stratigraphy. The PU at Akanani is largely uncontaminated by xenolithic material, and we have therefore excluded the published data in this regard from our discussion. The new data for the LMZ at Akanani are comparable to one sample from Overysel (data of Cawthorn et al., 1985). Samples from Overysel and Sandsloot (data of Harris & Chaumba, 2001; Pronost et al., 2008), however, report significantly higher Sr-initial ratios. The PU at Overysel (data of Cawthorn et al., 1985) reveals distinctly higher Sr-initial ratios in comparison to the Akanani data (although note that all of the Overysel samples were obtained from a restricted locality close to the granitic floor). These data were argued by Cawthorn et al. to be unaffected by footwall contamination. The data of Pronost et al. (2008) for the PU at Overysel, described as from a

contaminated sequence, reveals higher initial ratios in comparison to the Akanani data. Pronost et al. concluded that the Sr-isotope system in the Platreef "is more strongly perturbed" in localities where the floor is comprised of Archaean granite-gneiss (Overysel), as compared with the Sr-poor dolomite footwall (Sandsloot). We have excluded the isotopic data of Kruger (1990) from our comparisons as the samples are from Turfspruit, which as we noted earlier occurs in a separate subchamber. Moreover, Kruger (1990) described the samples as "mostly norite" and did not include a stratigraphic log.

In summary, we suspect that there are few regional differences in the Sr-isotopic ratios for the section described here i.e. Sandsloot, Zwartfontein, Overysel, and Akanani. The slightly lower Sr-isotopic ratio for the PU at Akanani may be a consequence of our sampling of a sequence not contaminated by xenoliths. The Sr initial ratio of the PU is not entirely dissimilar from the LMZ and the distinct geochemical break between the UCZ and the LMZ, so widely discussed from the eastern and western limbs (e.g., Sharpe, 1985; Kruger & Marsh, 1985; Kruger, 2005; Lee & Butcher, 1990), is not so apparent in the northern limb. The new data support earlier findings that both the PU (i.e. UCZ equivalent) and the LMZ have distinctly higher Sr-initial ratios in the northern limb as compared with the equivalent successions in the eastern and western limbs.

Nd Isotopic Systematics

The whole rock Nd isotopic data are presented in Table 3 (initial ratios were normalized to an age of 2.055 Ga). Averages for the new data are compared with averages of some published data in Table 4. The five samples of the LMZ from drill-hole ZF-1 have a relatively tightly constrained ε_{Nd} value (average of -6.73). Samples from the PU (excluding PU2)

report a lower ε_{Nd} value (average of -7.84), but with a noticeably poorer standard deviation. They yield a degree of scatter when plotted against the vertical log (Fig. 16). The three samples of the MMR are excluded from this average as they report a distinctly lower ε_{Nd} value (average of -11.35). We note that the ε_{Nd} value of one of the three samples is not dissimilar from the PU1 data; this may be due to some contamination (with earlier-formed PU1) in the basal part of this group of ultramafic layers. The three samples of the LCZ yield ε_{Nd} value (average of -6.85) similar to the LMZ. Plots of the Nd isotopic data against Zr reveal a degree of scatter (Fig. 15e, f). The four samples from drill-hole MO-3 (LMZ and PU) yield similar initial ratios to data from ZF-1. The new data are broadly comparable with data of Pronost et al. (2008) for the LMZ and PU from Overysel and Sandsloot (range of ε_{Nd} values of -6.2 through -9.6; average of -7.8, corrected for an age of 2.06 Ga). The Platreef data are also comparable to the Nd data of Maier et al. (2000) for broad sections of the RLS in the western limb, albeit the unusually low values associated with the MMR represent a new finding. The whole-rock isotopic data, however, need to be treated with some caution as Prevec et al. (2005) found evidence of marked mineral disequilibrium from Nd data for the Merensky Reef in the western limb (orthopyroxene ε_{Nd} values of -7.46 to -8.46; plagioclase ε_{Nd} values of -1.13 to -3.37).

Discussion

The classic cumulus theory, based on the concept of gravitative crystal settling (Wager & Brown, 1968), is no longer universally accepted. There is currently no consensus on an alternative mechanism for formation of igneous layering, although several possibilities have been suggested since the role of crystal settling in tholeiitic magmas was questioned (e.g., Bottinga & Weill 1970; McBirney & Noyes 1979; Naslund & McBirney 1996). Detailed

geochemical studies of the RLS, specifically of the UCZ in the western limb, led Eales et al. (1986; 1988) to suggest a hypothesis invoking *in situ* growth of crystals with multiple recharge events. Recharge was primarily ascribed to basal flows i.e., in the manner of Huppert and Sparks (1980). Volumetrically relatively small basal flows of ultramafic magma were implied to have subsequently mixed with much larger reservoirs of tholeiitic magma. This hypothesis also addressed formation of chromitite layers (Eales, 1987; Eales & Reynolds, 1987) and represented a major improvement on earlier concepts in which recharge of the Bushveld chamber was restricted to a handful of giant events (e.g., Wager & Brown, 1968; Sharpe, 1985; Von Gruenewaldt et al., 1985).

The mechanism of basal flows for the RLS has not, however, held up to close scrutiny, and despite us being amongst the original principal proponents of the model, we have realised there are serious flaws. The thermodynamics of flows which extend laterally for many tens of kilometres are problematic, particularly as regards maintaining the integrity of the upper contact with the postulated overlying magma reservoir. We would envisage a gradational boundary between the crystallization products of basal flows and the overlying resident magma (Mitchell et al., 2019a). The concept of a large convecting magma chamber may, in fact, be entirely inapplicable to the RLS, particularly when the relatively shallow crustal position is taken into account (Scoon & Mitchell, 2018). The maximum thickness of partially liquid material in the intrusive at any given time may have been less than a few tens of metres.

Field relationships are consistent with the RLS having formed by incremental emplacement of thousands of thin magma sheets (Scoon & Mitchell, 2012; 2018; Mitchell, 2019a) similar

to the growth mechanism of some granitic plutons (e.g., Miller et al., 2012). This hypothesis was favoured by geologists involved in regional mapping of the Bushveld Igneous Complex (e.g., Truter, 1955; Coertze, 1958; Schwellnus et al., 1962), i.e., prior to conceptualization of the RLS as a frozen magma chamber. The incremental build-up of layering is supported by the irregularity of the basal contact to the RLS (Fig. 4) and the sill-like shape of the eastern and western limbs (Scoon & Teigler, 1994; Mitchell et al., 2019a). The thickening of the RLS with depth at Akanani is consistent with the layering having built up incrementally, layer-by-layer. Attenuated sequences on the flanks of floor-rock domes reveal an extreme development of this offlap relationship (Marlowe & Van der Merwe, 1977; Sharpe & Chadwick, 1986; Uken & Watkeys, 1997; Scoon, 2002; Clarke et al., 2005). Floor rocks may have been highly mobile during emplacement of the RLS (Mitchell et al., 2019a). Early compartmentalization of the RLS is consistent with stratigraphic differences between subchambers (e.g., Sandsloot/Akanani and Turfspruit).

The floor contact of the RLS contrasts markedly with the planar nature of the roof contact with felsite of the Rooiberg Group. The absence of an upper chill (there is no Upper Border Group equivalent to the Skaergaard Intrusion) is significant. Felsite of the Rooiberg Group, the oldest component of the intrusion, reveals evidence of thermal metamorphism (Hall, 1932; Von Gruenewaldt, 1973), albeit the roof geometry is complicated by intrusion of the younger granites and granophyres (Cawthorn, 1998). The UZ, although widely interpreted as the fractionated residue of the underlying zones, may have crystallized from incremental addition of ferrobasaltic magmas sourced from deeper staging chambers (Scoon & Mitchell, 2012). These observations place important constraints on our understanding of the underlying zones, including the UCZ (and PU).

In a departure from the basal flow hypothesis, Mitchell (1996) and Mitchell and Scoon (2007) suggested pyroxenitic layers in the LMZ and UCZ, respectively, may have crystallized from magma injected as sills into a pre-existing (and already layered) noritic-anorthositic subsolidus cumulate sequence. Detailed documentation of inch-scale layering, i.e., in a pyroxenite layer located in the LMZ (western limb) and in the Merensky Reef (eastern limb) is consistent with the sills being linked to multiple pulses of magma. Each magma pulse may have thicknesses of only a few tens of cm. Chromitite layers may also be linked to the hypothesis of syn-magmatic sills (Voordouw et al., 2009; Mungall et al., 2016; Scoon & Costin, 2018). The two mechanisms of magma recharge, i.e., basal flows (or possibly more descriptively recharge of the resident magma) and syn-intrusive magma sheets should not, however, be seen as mutually exclusive (Scoon & Mitchell, 2018).

The Platreef Unit (PU) at Akanani is comprised of igneous layers far too complex to be interpreted as an upward-younging fractional crystallization sequence. We reconcile the new data to the hypothesis of multiple phases of magma recharge, including non-sequential replenishment by syn-intrusive sills, as presented by Mitchell & Scoon (2012). Within the constraints of this hypothesis, the PU1 subunit constitutes the primary stratigraphy. The PU1 subunit developed from magmas constrained within the ultramafic (U-type) and tholeiitic (A-type) lineages of Sharpe and Irvine (1983). We prefer to refer to the parental magma-types as lineages and do not subscribe to the popularly held view that there are a number of precisely-defined compositions. The incremental build up of the PU1 stratigraphy involved recharge by combinations of basal flows (mostly A-type) and magma sheets (mostly U-type). The height of the magma column was not sufficient to support bulk

mixing events and the layering is primarily constrained by the composition of the parental magmas. A huge range in parental magmas is suspected. The repetition of olivine- and chromite-rich layers in the ZF-1 stratigraphy (Fig. 5) supports the concept of multiple episodes of magma replenishment by U-type magmas, possibly picritic compositions, as discussed by Scoon & de Klerk (1987) in context of the interval containing the UG2, Pseudo Reefs and Merensky Reef in the western limb.

The younger PU2 subunit was suggested by Mitchell & Scoon (2012) to have been emplaced as a series of sinuous lenses or sills into the older, and already complexly-layered, PU1 subunit. This mechanism is similar to that proposed by Bédard et al. (1988) for the harzburgite layers in the Rum Intrusion, Scotland. The PU3 subunit was interpreted by Mitchell & Scoon (2012) as reconstituted (recrystallized) earlier-formed lithologies. Recrystallization is ascribed to heat associated with multiple intrusions during build up of the PU1 subunit and the later emplacement of the PU2 sills.

Evidence of fractional crystallization within the ZF-1 stratigraphy is restricted to the broad zonal framework. The LCZ is relatively primitive and the LMZ is relatively fractionated. These zones can also be ascribed to variants of the U- and A-magma lineages, respectively, as discussed by Eales (2002) for the western/eastern limbs. The PU reveals intermediate compositions, a feature which is consistent with the UCZ from the western/eastern limbs. We should point out that the UCZ-LMZ contact, at least in the western limb, is a geochemical continuum rather than the sharp break envisaged by many (Mitchell, 1990). Similarities between the olivine-rich lithologies of the PU2 subunit at Akanani and the Pseudo Reefs of the UCZ were described earlier. The bifurcation of the multiple layers of

harzburgite in the Pseudo Reef unit along strike in the Swartklip facies, together with the occurrence of magmatic-reaction chromite stringers on their upper and lower contacts offers compelling evidence of syn-intrusive sills (Mitchell et al., 2019a).

A necessary caveat to understanding the UCZ (and the LCZ) is the problem of the chromium budget. U-type magmas charged with phenocrysts of Cr-spinel (Eales, 2000), sufficiently abundant in some instances as to form crystal slurries (Eales, 2002), were most likely sourced from deeper staging chambers (Eales and Costin, 2012). Chromitites are relatively scarce in the PU, but the occurrence of thin chromite stringers at Akanani is of interest. We restrict ourselves to suggesting the unusual, amoeboidal textures of some of the Cr-spinel grains are indicative of several stages of growth and re-equilibration, i.e., consistent with multiple replenishment events. Yudovskaya et al. (2019) came to a similar conclusion from a more detailed study of similar Cr-spinels from the Turfspruit locality.

The new isotopic data for the Akanani section are consistent with the concept of multiple recharge events (Fig. 17). Each zone i.e. LCZ, PU, and LMZ is ascribed to recharge by isotopically-distinct magmas i.e. LCZ (U-type), PU (U- and A- types), and LMZ (A-type). The A-type magmas within the PU1 subunit are isotopically-distinct from those associated with the LMZ, yet crystallized noritic lithologies which are petrographically (and macroscopically) broadly similar. In the western and eastern limbs, the norite from the LMZ is discriminated from the norite of the UCZ by the paucity in the Cr content (Mitchell, 1990), but whether this is broadly applicable we are unsure. The anomalously high Sr-initial ratio of the PU (in comparison to the UCZ of the eastern and western limbs) is probably a primary feature (and is unrelated to footwall contamination), a conclusion also reached by Cawthorn et al. (1985).

The unusually high Sr-initial ratio of all three zones investigated at Akanani may indicate this is a regional feature of the northern limb. The range in ε_{Nd} values is consistent with multiple injections of three or more discrete magma-lineages. The complexity of the RLS is such that we cannot pinpoint all of the parental magmas. Recharge from deeper staging chambers implies an almost unlimited compositional variation within the constraint of the generic U- and A-type lineages. This interpretation may explain the scatter in the Sr initial ratio within the PU1 subunit, i.e., exclusive of complexities introduced by intrusion of the later PU2 sills and recrystallization of the PU3 lithologies. Partial melting of earlier-formed PU1 lithologies *in situ*, triggered by persistent magma recharge during development of the PU1 stratigraphy, as well as associated with emplacement of the PU2 sills, adds an additional complexity (Mitchell et al., 2019a). Moreover, each magma pulse may have contained varying proportions of phenocrysts (including Cr-spinel and olivine in the picritic magmas), which adds another complexity to unravelling parental magmas.

A comparison of the Akanani isotopic data with averages for the lithosphere defined by Zindler & Hart (1986) emphasizes these differences (Fig. 17). The LCZ may be associated with magma derived from an Enriched Mantle 1 source. The PU1 and LMZ may be associated with magma derived from an Enriched Mantle 2 source with varying degrees of crustal contamination. Contamination occurred in deeper staging chambers.

The possibility of the general upward-fractionation in the RLS being related to progressive contamination (Maier et al., 2000) is consistent with the new data presented here, with the exception of the data pertaining specifically to the MMR. The variation in the Sr initial ratio of the PU1 (and relatively tightly constrained ε_{Nd} value), as compared with the LMZ,

indicates this part of the stratigraphy (i.e., associated with the most complexly layered section of the stratigraphy) reflects far greater degrees of crustal contamination (Fig. 17). Moreover, the relatively low Sr-initial ratios of some samples from the PU1 subunit may suggest an enriched mantle source (EM2), with the higher initial ratios consistent with a trend towards a depleted mantle source (DM).

The parental magma associated with the MMR reports an anomalously high Sr initial ratio and a markedly low ε_{Nd} value. The olivine-saturated and unusually PGE-rich parental magma associated with the MMR was derived from a localized mantle source (EM1). The mantle source may have been anomalously rich in garnet-peridotite (e.g., Wasch et al., 2009). This melt has, however, appeared to have experienced a greater degree of crustal contamination than the parental magmas associated with the PU1 subunit and the LMZ. The isotopic data for the MMR are broadly similar to the findings of Prevec et al. (2016) from a study of the Merensky Reef in the eastern limb. Both studies are, however, of a preliminary nature and additional data are required to confirm these trends.

A localized mantle-source (EM1) can also be envisaged for the two samples of harzburgite from the LCZ at Akanani. The low Sr initial ratio and low ε_{Nd} values are consistent with relatively low levels of crustal contamination. The possibility of olivine-rich magmas being derived from a mantle source, with little influence from a crustal staging chamber, may explain why the harzburgites at this height in the stratigraphy are either barren or poorly mineralized.

Conclusions

We have not commented on the origin of mineralization in the Platreef Unit as our study is primarily directed at unravelling the complexities of the layering. A necessary caveat to formation of PGE-rich orebodies in the RLS may, however, be derivation of unusual, olivine-saturated magmas from a mantle source. Most recent studies, including the Re-Os and S isotopic study of Yudovskaya et al. (2017b), also indicate the importance of orthomagmatic processes. We conclude that some PGE-rich orebodies (e.g., Platreef and Merensky Reef) are related to ultramafic magmas injected as syn-magmatic sills into an already complexly-layered substrate. The unique isotopic fingerprint of the PGE-rich parental magma associated with these specific orebodies reflects the unusual combination of a localized mantle source and a high degree of crustal contamination. The interpretation of reef-style deposits as orthomagmatic sills has important consequences for both current and future mining operations.

Acknowledgements

Sampling and additional logging of drill-holes in support of our earlier study was undertaken with the assistance of Lonplats. In this regard, we thank Godfrey Ndluvu for his support. Financial support from Rhodes University for the electron microprobe analyses is acknowledged. The isotopes were partly funded by RNS and partly by the French Government Laboratory of Excellence initiative ANR-10-LABX-0006. Reviews by Marina Yudovskaya and Christian Ihlenfeld were both constructive and extremely helpful, as was the editorial assistance of Andreas Audetat and Marjorie Wilson.

References

Armitage, P.E.B., McDonald, I., Edwards, S.J., & Manby, G.M. (2001). Platinum-group element mineralization in the Platreef and calc-silicate footwall at Sandsloot, Potgietersrus district, South Africa. *Transactions of the Institute of Mining and Metallurgy* **111**, B36-B45.

Bédard, J. H., Sparks, R. S. J., Renner, R., Cheadle, M. J. & Hallworth, M. A. (1988). Peridotite sills and metasomatic gabbros in the Eastern Layered Series of the Rhum complex. *Journal of the Geological Society* **145**, 207-224.

Bottinga, Y. & Weill, D.F. (1970). Densities of liquid silicate systems calculated from partial molar volumes of oxide components. *American Journal of Science* **372**, 438-475.

Buchanan, D.L., Nolan, J., Suddaby, P., Rouse, J.E., Viljoen, M.J. & Davenport, J.W.J. (1981). The genesis of sulphide mineralization in a portion of the Potgietersrus limb of the Bushveld Complex. *Economic Geology* **76**, 568-579.

Cawthorn R.G. (1998). Geometrical relations between the Transvaal Supergroup, the Rooiberg Group and the mafic rocks of the Bushveld Complex. *South African Journal of Geology* **101**, 275–280.

Cawthorn R.G. (2013). The residual or roof zone of the Bushveld Complex. *Journal of Petrology* **54**, 1875–1900.

Cawthorn, R.G., Barton, J.M., & Viljoen, M.J. (1985). Interaction of floor rocks with the Platreef on Overysel, Potgietersrus, Northern Transvaal. *Economic Geology* **80**, 988-1006.

Cawthorn, R.G. & Walraven, F. (1998). Emplacement and crystallization time for the Bushveld Complex. *Journal of Petrology* **39**, 1669-1687.

Clarke BM, Uken R, Watkeys, MK, Reinhardt, J. (2005). Folding of the Rustenburg Layered Suite adjacent to the Steelpoort Pericline: implications for syn-Bushveld tectonism in the eastern Bushveld Complex. *South African Journal of Geology* **108**, 397-412.

Clarke, B.M., Uken R., & Reinhardt, J. (2009). Structural and compositional constraints on the emplacement of the Bushveld Complex, South Africa. *Lithos* **111**, 21–36.

Coertze, F.J. (1958). Intrusive relationships and ore deposits in the western part of the Bushveld Igneous Complex. *Transactions Geological Society South Africa* **61**, 387-392.

Eales, H. V. (1987). Upper Critical Zone chromitite layers at R.P.M. Union Section Mine, western Bushveld Complex. In: Stowe, C.W. (Ed.) *Evolution of chromite ore fields.* Van Nostrand Reinhold, New York, 144-168.

Eales, H. V. (2000). Implications of the chromium budget of the Western limb of the Bushveld Complex. *South African Journal of Geology* **103**, 141-150.

Eales, H.V. (2002). Caveats in defining the magmas parental to the mafic rocks of the Bushveld Complex, and the manner of their emplacement: review and commentary. *Mineralogical Magazine* **66**, 815-832.

Eales H.V. & Costin G. (2012). Crustally contaminated komatiite: primary source of the chromitites and marginal, lower, and critical zone magmas in a staging chamber beneath the Bushveld Complex. *Economic Geology* **107**, 645–665.

Eales, H.V., Field, M., De Klerk, W.J. & Scoon, R.N. (1988). Regional trends of chemical variation and thermal erosion in the Upper Critical Zone, western Bushveld Complex. *Mineralogical Magazine* **52**, 63-79.

Eales, H.V., Marsh, J.S., Mitchell, A.A., de Klerk, W.J., Kruger, F.J. & Field, M. (1986). Some geochemical constraints upon models for the crystallization of the upper Critical Zone-Main Zone interval, northwestern Bushveld Complex. *Mineralogical Magazine* **50**, 567-582.

Eales, H.V. & Reynolds, I.M. (1986). Cryptic variations within chromitites of the Upper Critical Zone, north-western Bushveld Complex. *Economic Geology* **81**, 1056-1066.

Gain, S.B. & Mostert, A.B. (1982). The geological setting of the platinoid and base metal sulphide mineralization in the Platreef of the Bushveld Complex in Drenthe, north of Potgietersrus. *Economic Geology* **77**, 1395-1404.

Grobler, D.F., Brits, J.A.N., Maier, W.D., & Crossingham, A. (2019). Litho- and chemostratigraphy of the Flatreef PGE deposit, northern Bushveld Complex. *Mineralium Deposita* **54**, 3–28

Hall, A.L. (1932). The Bushveld Igneous Complex of the central Transvaal. *Geological Survey of South Africa Memoir* **28**, 560 p.

Harris, C. & Chaumba, J.B. (2001). Crustal contamination and fluid-rock interaction during formation of the Platreef, northern limb of the Bushveld Complex, South Africa. *Journal of Petrology* **44**, 1321-1347.

Hatton, C.J. & Schweitzer, J.K. (1995). Evidence for synchronous extrusive and intrusive Bushveld magmatism. *Journal of African Earth Sciences* **21**, 579-594.

Holwell, D.A., Armitage, P.E.B., & McDonald, I. (2005). Observations on the relationship between the Platreef and its hangingwall. *Transactions of the Institute of Mining and Metallurgy* **114**, B199-B207.

Holwell, D.A., Boyce, A.J., & McDonald, I. (2007). Sulfur Isotope Variations within the Platreef Ni-Cu-PGE Deposit: Genetic Implications for the Origin of Sulfide Mineralization. *Economic Geology* **102**, 1091–1110.

Holwell, D.A. & Jordaan, A. (2006). Three-dimensional mapping of the Platreef at the Zwartfontein South mine: implications for the timing of magmatic events in the northern

limb of the Bushveld Complex. *Transactions of the Institute of Mining and Metallurgy* **115**, B41-B48.

Huppert, H.E. and Sparks, R.S.J. (1980). The fluid dynamics of a basaltic magma chamber replenished by influx of hot, dense ultrabasic magma. *Contributions to Mineralogy and Petrology* **75**, 279-289.

Hutchinson, D. & Kinnaird, J.A. (2005). Complex multi-stage genesis for the Ni-Cu-PGE mineralization in the southern region of the Platreef, Bushveld Complex, South Africa. *Transactions of the Institute of Mining and Metallurgy* **114**, B208–B224.

Kinnaird, J.A., Hutchinson, D., Schurmann, L., Nex, P. & De Lange, R. (2005). Petrology and mineralization of the southern Platreef: northern limb of the Bushveld complex, South Africa. *Mineralium Deposita* **40**, 576-597.

Kruger FJ (2005). Filling the Bushveld Complex magma chamber: lateral expansion, roof and floor interaction, magmatic unconformities, and the formation of giant chromitite, PGE and Ti–V–magnetitite deposits. *Mineralium Deposita* **40**, 451–472.

Kruger, F.J. & Marsh, J.S. (1982). Significance of $^{87}Sr/^{86}Sr$ ratios in the Merensky cyclic unit of the Bushveld Complex. *Nature* **298**, 53-55.

Latypov, R., Chistyakova, S. & Kramers, J. (2017). Arguments against syn-magmatic sills in the Bushveld Complex, South Africa. *South African Journal of Geology* **120**, 565-574.

Lee, C.A. & Butcher, A.R. (1990). Cyclicity in the Sr isotope stratigraphy through the Merensky and Bastard Reef Units, Atok Section, eastern Bushveld Complex. *Economic Geology* **85**, 877-883.

Maier W.D., Arndt N.T. & Curl E.A. (2000). Progressive crustal contamination of the Bushveld Complex: evidence from Nd isotopic analyses of the cumulate rocks: *Contributions to Mineralogy and Petrology* **140**, 316–327.

Marlow, A. G. & Van der Merwe, M.J. (1977). The geology and potential economic significance of the Malope area, northeastern Bushveld Complex. *Geological Society of South Africa Transactions* **80**, 117-123.

McBirney, A.R. & Noyes, R.M. (1979). Crystallization and layering of the Skaergaard Intrusion. *Journal of Petrology* **20**, 487-554.

McDonald, I., Holwell, D.A. & Armitage, P.E.B. (2005). Geochemistry and mineralogy of the Platreef and "Critical zone" of the northern lobe of the Bushveld Complex, South Africa: implications for Bushveld stratigraphy and the development of PGE mineralization. *Mineralium Deposita* **40**, 526-549.

McDonald, I. & Holwell, D.A. (2011). Geology of the Northern Bushveld Complex and the setting and genesis of the Platreef Ni-Cu-PGE deposit. *Reviews in Economic Geology* **107**, 713-722.

Miller, C.F., Furbish, D.J., Walker, B.A., Claiborne, L.L., Koteas, G.C., Bleick, H.A. & Miller, J.S. (2011). Growth of plutons by incremental emplacement of sheets in crystal-rich host. Evidence from Miocene intrusions of the Colorado River region, Nevada, USA. *Tectonophysics* **500**, 65–77.

Mitchell, A. A. (2006). A Review of the Geology of the Platreef on the Akanani Properties, with Particular Emphasis on the Southern Priority Area. *Unpublished Internal Report, Afriore*, 15 p.

Mitchell, A. A. (1990). The stratigraphy, petrography and mineralogy of the Main Zone of the north-western Bushveld Complex. *South African Journal of Geology* **93**, 818-831.

Mitchell, A. A. (1996). Compositional cyclicity in a pyroxenitic layer from the Main Zone of the western Bushveld Complex: evidence for repeated magma flux. *Mineralogical Magazine* **60**, 149-161.

Mitchell, A.A., Eales, H.V. & Kruger, F.J. (1998). Magma replenishment, and the significance of poikilitic textures, in the Lower Main Zone of the western Bushveld Complex, South Africa. *Mineralogical Magazine* **62**, 435-450.

Mitchell, A.A., Henckel, J. & Mason-Apps, A. (2019b). The Upper Critical Zone of the Rustenburg Layered Suite in the Swartklip Sector, north-western Bushveld Complex, on the farm Wilgerspruit 2JQ: I. Stratigraphy and PGE mineralization patterns. *South African Journal of Geology* 122, 117-142. https://doi.org/10.25131/sajg.122.0010

Mitchell, A.A. & Scoon, R.N. (2007). The Merensky Reef at Winnaarshoek, Eastern Bushveld Complex: a primary magmatic hypothesis based on a wide reef facies. *Economic Geology* **102**, 971-1009.

Mitchell, A.A. & Scoon, R.N. (2012). The Platreef of the Bushveld Complex, South Africa: a model of multiple, non-sequential magma replenishment based on observations at the Akanani Project. *South African Journal of Geology* **115**, 535-550.

Mitchell, A.A., Scoon, R.N. & Sharpe, M.R. (2019a). The Upper Critical Zone in the Swartklip Sector, north-western Bushveld Complex, on the farm Wilgerspruit 2JQ: II. Origin by intrusion of ultramafic sills with concomitant partial melting of host norite-anorthosite cumulates. *South African Journal of Geology* 122, 143-162. https://doi.org/10.25131/sajg.122.0011

Mungall, J.E., Kamo, S.L. & McQuade, S. (2016.) U–Pb geochronology documents out-of-sequence emplacement of ultramafic layers in the Bushveld Igneous Complex of South Africa. *Nature Communications* **7:13385**, 1-13.

Naslund, H.R. & McBirney, A.R. (1996). Mechanisms of formation of igneous layering. In: *Layered Intrusions, Amsterdam, Elsevier*, 1-44.

Pin, C., Briot, D., Bassin, C. & Poitrasson, F. (1994). Concomitant separation of strontium and samarium-neodymium for isotopic analysis in silicate samples, based on specific extraction chromatography. *Analytica Chimica Acta* **298**, 209–217.

Pin, C. & Zalduegui, J.S. (1997). Sequential separation of light rare-earth elements, thorium and uranium by miniaturized extraction chromatography: Application to isotopic analyses of silicate rocks. *Analytica Chimica Acta* **339**, 79–89.

Prevec S.A., Ashwal L.D., & Mkaza M.S. (2005). Mineral disequilibrium in the Merensky Reef, western Bushveld Complex, South Africa: new Sm–Nd isotope evidence. *Contributions to Mineralogy and Petrology* 149, 306–315

Prevec, S.A., Scoon, R.N. & Raines, M.D. (2016). Sm-Nd isotopic evidence for sampling of multiple sources during the emplacement of the Upper Critical Zone, Bushveld Complex, South Africa (abstract). *35th IGC, Cape Town*.

Pronost, J., Harris, C. & Pin, C. (2008). Relationship between footwall composition, crustal contamination, and fluid–rock interaction in the Platreef, Bushveld Complex, South Africa. *Mineralium Deposita* **43**, 825-848.

Schwellnus, J.S.I., Engelbrecht, L.N.J., Coertze, F.J., Russell, M.D., Maherbe, S.J., Van Rooyen, D.P. & Cooke, R. (1962). The geology of the Olifants River area, Transvaal. *Geological Survey of South Africa Explanation Sheets 2429B and 2430A*, 87 p.

Scoates, J. S. & Friedman, R. M. (2008). Precise Age of the Platiniferous Merensky Reef, Bushveld Complex, South Africa, by the U-Pb Zircon Chemical Abrasion ID-TIMS Technique. *Economic Geology* **103**, 465-471.

Scoon, R.N. (2002). A new occurrence of Merensky Reef on the flanks of the Zaaikloof dome, northeastern Bushveld Complex: Relationship between diapirism and magma replenishment. *Economic Geology* **97**, 1037-1049.

Scoon, R.N. & Costin, G. (2018). Chemistry, morphology and origin of magmatic-reaction chromite stringers associated with anorthosite in the Upper Critical Zone at Winnaarshoek, eastern limb of the Bushveld Complex. *Journal of Petrology* **59**, 1551–1578.

Scoon, R.N. & De Klerk, W.J. (1987). The relationship of olivine cumulates and mineralization to cyclic units in part of the Upper Critical Zone of the western Bushveld Complex. *Canadian Mineralogist* **25**, 51-77.

Scoon R. N. and Mitchell A. A. (2012). The Upper Zone of the Bushveld Complex at Roossenekal: Geochemical Stratigraphy and Evidence of Multiple Episodes of Magma Replenishment. *South African Journal of Geology* **115**, 515-534.

Scoon, R.N. & Mitchell, A.A. (2018). Discussion of "Arguments against Syn-magmatic Sills in the Bushveld Complex, South Africa" by R. Latypov, S. Chistyakova and J. Kramers. *South African Journal of Geology* **121**, 201-210.

Scoon, R.N. & Teigler, E.B. (1994). Platinum-group element mineralization in the Critical Zone of the western Bushveld Complex: I. Sulfide-poor chromitites below the UG-2. *Economic Geology* **89**, 1094-1121.

Sharman-Harris, E.R., Kinnaird, J.A., Harris, C. & Horstman, U.E. (2005). A new look at sulphide mineralization of the northern limb, Bushveld complex: a stable isotope study. *Applied Earth Sciences, Transactions Institute Mining and Metallurgy* **114,** B252-263.

Sharpe, M.R. (1981). The chronology of magma influxes to the eastern compartment of the Bushveld Complex as exemplified by its marginal border groups. *Geological Society of London Journal* **138**, 307-326.

Sharpe, M.R. (1985). Strontium isotope evidence for preserved density stratification in the eastern Bushveld Complex. *Nature* **316**, 119-126.

Sharpe, M.R. & Chadwick, B. (1982). Structures in Transvaal Sequence rocks within and adjacent to the eastern Bushveld Complex. *Transactions of the Geological Society of South Africa* **85**, 29-41.

Sharpe, M.R. & Irvine, T.N. (1983). Melting relations of two Bushveld chilled margin rocks and implications for the origin of chromitite. *Carnegie Institute Washington Yearbook* **82**, 295-300.

South African Committee for Stratigraphy (1980). Stratigraphy of South Africa, Part I (Compiler L.E. Kent). *Geological Survey of South Africa Handbook* **8**, 690 p.

Teigler, B. & Eales, H.V. (1996). The Lower and Critical zones of the western limb of the Bushveld Complex as intersected by the Nooitgedacht boreholes. *Geological Survey of South Africa Bulletin* **111**, 126 p.

Truter, F.C. (1955). Modern concepts of the Bushveld Igneous Complex. *First Meeting Southern Regional Committee for Geology (CCTA) Harare, Zimbabwe*, 77-91.

Uken, R. & Watkeys, M.K. (1997). Diapirism initiated by the Bushveld Complex, South Africa. *Geology* **25**, 723-726.

Van der Merwe, M.J. (1976). The layered sequence of the Potgietersrus Limb of the Bushveld Complex. *Economic Geology* **71**, 1337-1351.

Viljoen, M. J. (2008). The nature and thoughts on the origin of the Platreef PGE bonanza (Abstract). SEG-GSSA Conference "Africa Uncovered: mineral resources for the future", 146-147.

Viljoen, M. J. (2016). The Bushveld Complex: Host to the worlds' largest platinum, chromium and vanadium resources. In: Wilson, M.G.C. & Viljoen, R.P. (Eds.), The Great Mineral Fields of Africa. *Episodes* **39(2)**, 239-268.

Viljoen, M.J. and Schürmann, L.W. (1998). Platinum-group metals. In: Wilson, M.G.C. and Anhaeusser, C.R. (ed.) "The Mineral Resources of South Africa Handbook". *Council for Geoscience* **16**, 532-568.

Viljoen, M.J., Theron, J., Underwood, B., Walters, B.M., Weaver, J. & Peyerl, W. (1986). The Amandelbult Section of Rustenburg Platinum Mines Limited, with reference to the Merensky Reef, in Anhaeusser, C.R. & Maske, S. (Eds.), *Mineral Deposits of Southern Africa: Johannesburg, Geological Society of South Africa* **2**, 1041-1060.

Von Gruenewaldt, G., Sharpe, M.R., & Hatton, C.J. (1985). The Bushveld Complex: Introduction and review. *Economic Geology* **80**, 803-812.

Voordouw R., Gutzmer J. & Beukes N.J. (2009). Intrusive origin for Upper Group (UGI, UG2) stratiform chromitite seams in the Dwars River area, Bushveld Complex, South Africa. *Mineralogy and Petrology* **97**, 75–94.

Wagner, P.A. (1929). The Platinum Deposits and Mines of South Africa. *Oliver & Boyd, Edinburgh* 326 p.

Walraven, F.J., Armstrong, R.A., & Kruger, F.J. (1990). A chronostratigraphic framework for the north-central Kaapvaal craton, the Bushveld Complex and Vredefort structure. *Tectonophysics* **171**, 23-48.

Walraven F.J. & Hattingh E. (1993). Geochronology of the Nebo Granite, Bushveld Complex. *South African Journal of Geology* **96**, 31-41.

Wasch, L. J., Van der Zwan, F. M., Nebel, O., Morel, M. L. A., Hellebrand, E. W. G., Pearson, D. G. & Davies, G. R. (2009). An alternative model for silica enrichment in the Kaapvaal subcontinental lithospheric mantle. *Geochimica et Cosmochimica Acta*, **73**, 6894–6917.

White, J.A. (1994). The Potgietersrus Prospect – Geology and exploration history: *15th CMMI Congress, Johannesburg, SAIMM* **3**, 173-181.

Wilson, A.H. (2012). A Chill Sequence to the Bushveld Complex: Insight into the First Stage of Emplacement and Implications for the Parental Magmas. *Journal of Petrology* **53**, 1123-1168.

Yudovskaya M., Belousova E., Kinnaird J., Dubinina E., Grobler D.F., Pearson N. (2017b). Re-Os and S isotope evidence for the origin of Platreef mineralization (Bushveld Complex) *Geochimica Cosmochimica Acta* **214**, 282-307.

Yudovskaya, M.A., Costin, G., Shilovskikh, V., Chaplygin, I., McCreesh, M. & Kinnaird, J. (2019). Bushveld symplectic and sieve-textured chromite is a result of coupled dissolution-reprecipitation: a comparison with xenocrystic chromite reactions in arc basalt. *Contributions to Mineralogy and Petrology* **174:74**, 21 p.

Yudovskaya M.A., Kinnaird J.A., Grobler D.F., Costin G., Abramova V.D., Dunnett T., Barnes, S. (2017a). Zonation of Merensky-Style Platinum-Group Element Mineralization in Turfspruit Thick Reef Facies (Northern Limb of the Bushveld Complex). *Economic Geology* **112**, 1333-1365.

Yudovskaya, M.A., Kinnaird, J.A., Sobolev, A.V., Kuzmin, D.V., McDonald, I. & Wilson, A.H. (2013). Petrogenesis of the lower zone olivine-rich cumulates beneath the Platreef and their correlation with recognized occurrences in the Bushveld Complex. *Economic Geology* **108**, 1923–1952.

Zeh, A., Ovtcharova, M., Wilson, A.H. & Schaltegger, U. (2015). The Bushveld Complex was emplaced and cooled in less than one million years – results of zirconology, and geotectonic implications. *Earth and Planetary Science Letters* **418**, 103–114.

Zindler, A., & Hart, S.R. (1986). Chemical geodynamics. *Annual Review Earth Planetary Science* **14**, 493–571.

List of Figures

Fig. 1. Regional map of the Bushveld Igneous Complex showing location of Akanani in the northern limb. The Rustenburg Layered Suite has cut down through metasediments of the Transvaal Supergoup into granite of the cratonic basement. The older felsites of the Rooiberg Group and younger granite-granophyre of the Lebowa Granite Suite occur in the centre of the Transvaal basin. Simplified from the 1:1,000,000 scale map published by the Council for Geoscience.

Fig. 2. (a) View of the Akanani Leasehold overlooking the open pit at the Mogalakwena platinum mine (Sandsloot). The paucity of outcrop on the interior plateau of southern Africa is characteristic. Low hills in the centre are associated with resistant gabbronorite of the Upper Main Zone; (b) Section of a contaminated and folded section of the Platreef orebody overlain by the Lower Main Zone and cut by a younger dolerite dyke at the Overysel platinum mine (Photograph and labelling of Viljoen, 2016).

Fig. 3. Simplified geological map showing location of Akanani Leasehold (Zwartfontein 814 LR and Moordkopje) and location of drill-holes studied here. Also shown are the open pit mines on up-dip properties of Sandsloot, Vaalkop, Zwartfontein 818LR, and Overysel. The Rustenburg Layered Suite rests on dolomite of the Transvaal Supergroup in the southern part of the area and on Archaean granite-gneiss in the northern part. Simplified from the 1:250,000 scale maps (2328 and 2428) published by the Council for Geoscience.

Fig. 4. (a) Generalized stratigraphic column for the eastern limb of the Bushveld Igneous Complex showing subdivision of the Rustenburg Layered Suite into zones; (b) Schematic

section of the Northern Limb at Akanani aligned with drill-hole ZF-1, Zwartfontein 814 LR. Interpretation based on the 1:250,000 scale map 2328 published by the Council for Geoscience and drilling at Akanani and based on correlation of the Platreef Unit with the UCZ.

Fig. 5. Stratigraphic log for drill-hole ZF-1 showing basal part of the Lower Main Zone (LMZ), Platreef Unit, and upper part of the Lower Critical Zone (LCZ). Sample positions annotated relative to depth. Occurrence of olivine, Cr-spinel, and lithologies with a pegmatoidal texture highlighted. Lithologies simplified in parts of column due to scale constraints. The proportion of orthopyroxene and clinopyroxene is variable and the subordinate presence of clinopyroxene-rich lithologies is denoted by brackets. Grouping of lithologies into the PU1, PU2 and PU3 subunits is interpretative. Identification of the Main Mineralized Reef (MMR) and Lower Reefs (LR1-3) is for descriptive purposes and has no bearing on potentially mineable orebodies.

Fig. 6. The contact between norite of the Lower Main Zone and the distinctly more mafic Platreef Unit occurs at a depth of 1013.71 m in drill-hole ZF-1. Average grades of 4.02 g/t over a width of 56.29 m, and 6.32 g/t over a width of 4.01 m, are for 3PGE+Au using base of the Lower Main Zone as datum selected by the mining company.

Fig. 7. (a) A richly mineralized layer of poikilitic feldspathic harzburgite (centre), with large oikocrysts of orthopyroxene in a black matrix of serpentinized olivine, is bounded by layers of recrystallized olivine orthopyroxenite (upper and lower), Main Mineralized Reef in drill-hole ZF-3, Akanani (from Mitchell & Scoon, 2012a). Samples ZF-3/34 and ZF-3/36 report

mining assays of 10.52 g/t and 16.94 g/t (3PGE+Au); (b) Feldspathic orthopyroxenite from the PU reveals patchy development of pegmatoid (sample ZF-1/1096.8); (c) Chromite stringer from the PU (sample ZF-1/1097.2c) enclosed by orthopyroxenite (sample ZF-1/1097.2b,d) with irregular development of notably more plagioclase-rich pegmatoid (sample ZF-1/1097.2a,e); (d) Partially serpentinized poikilitic harzburgite from the LCZ reveals light grey mottles of orthopyroxene (sample ZF-1/1111.2).

Fig. 8. The vertical distribution of Pt, Pd, Rh, and Au, the Pt/Pd ratio, and the whole-rock Co content in drill-hole ZF-1 define four mineralized "reefs". Data based on commercial assays provided by the mining company.

Fig. 9. (a) Feldspathic orthopyroxenite with coarse, cumulus grains of orthopyroxene (Opx) and interstitial clinopyroxene (Cpx) and plagioclase (Pl) (sample ZF-1/1097.2b); (b) Closely-packed grains of orthopyroxene reveal triple junctions in a layer of orthopyroxenite located proximal to a chromite stringer (sample ZF-1/1097.2c); (c) Large grains of oikocrystic orthopyroxene enclose earlier-formed grains of Cr-spinel and amphibole (Amp) (sample ZF-1/1097.2d); (d) Chromite stringer with small rounded grains of Cr-spinel (Chr) together with interstitial orthopyroxene (Opx) and subordinate biotite (BI) (sample ZF-1/1097.2c); (e) Oikocrysts of orthopyroxene (Opx 2) enclose an earlier generation of orthopyroxene (Opx 1) and earlier-formed Cr-spinel (sample ZF-1/1097.2c); (f) Orthopyroxene with exsolved clinopyroxene (sample ZF-1/1097.2d). All samples from the PU. Photomicrographs a-b in plane polarised light and c-f with crossed polarisers.

Fig. 10. (a-b) A thin chromite stringer from the PU is comprised of rounded grains of Cr-spinel with silicate cores dominated by orthopyroxene (Opx) and amphibole (Am) (sample ZF-1/1097.2); (c-d) Small, irregular inclusions of silicates in euhedral grains of Cr-spinel (sample ZF-1/1097.2c). Photomicrographs a-b with crossed polarisers and c-d in plane polarised light.

Fig. 11: Coalesced grains of Cr-spinel from a chromite stringer in the PU reveal silicate inclusions (sample ZF-1/1097.2c). Photomicrographs with crossed polarisers.

Fig. 12. (a) Harzburgite from the LCZ reveals grains of olivine (Ol) and clinopyroxene (Cpx) enclosed by oikocrystic orthopyroxene (Opx), together with disseminated Cr-spinel (Chr) (sample ZF-1/1111.2); (b) The harzburgite from the LCZ is invariably partially serpentinized (sample ZF-1/1111.2). Photomicrographs with crossed polarisers.

Fig. 13. Plot of Sr against Y and Rb based on whole-rock compositions for samples from drill-hole ZF-1.

Fig. 14. Selected trace elements plotted against Zr based on whole-rock compositions for samples from drill-hole ZF-1.

Fig. 15. Selected trace elements plotted against Zr based on whole-rock compositions for samples from drill-hole ZF-1.

Fig. 16. Plot of the Sr-initial ratio and the ε_{Nd} value against height for samples from drill-hole ZF-1.

Fig. 17. Plot of the Sr-initial ratio against the ε_{Nd} value for samples from drill-hole ZF-1. Fields labelled DMM (Depleted Mantle), HIMU, EM1 (Enriched Mantle 1) and EM2 (Enriched Mantle 2) after Zindler & Hart (1986). The general trend suggests an extremely enriched mantle source, characteristic for old, recycled lithospheric mantle.

Table 1: List of Samples

Drill Hole	Depth (m)	Zone/Unit	Subunit	Lithology	Texture	Notes	PGE	Reef
ZF-1	1001.5	Lower Main	LMZ	Norite	Coarse-grained		Barren	
ZF-1	1005.7	Lower Main	LMZ	Norite	Coarse-grained		Barren	
ZF-1	1010.2	Lower Main	LMZ	Norite	Coarse-grained		Barren	
ZF-1	1011.8	Lower Main	LMZ	Norite	Coarse-grained		Barren	
ZF-1	1012.8	Lower Main	LMZ	Norite	Coarse-grained		Barren	
ZF-1	1016.2	Platreef	PU1	Feldspathic Orthopyroxenite	Medium-grained		Weakly mineralized	
ZF-1	1019.3	Platreef	PU1	Feldspathic Orthopyroxenite	Medium-grained		Weakly mineralized	
ZF-1	1022.6	Platreef	PU2	Orthopyroxenite	Medium-grained		Richly mineralized	MMR
ZF-1	1025.1	Platreef	PU2	Feldspathic Harzburgite	Medium-grained		Richly mineralized	MMR
ZF-1	1026.0	Platreef	PU2	Feldspathic Harzburgite	Medium-grained		Richly mineralized	MMR
ZF-1	1027.8	Platreef	PU1	Melanorite	Medium-grained		Weakly mineralized	
ZF-1	1033.3	Platreef	PU1	Feldspathic Orthopyroxenite	Medium-grained		Weakly mineralized	
ZF-1	1039.6	Platreef	PU1	Melanorite	Medium-grained		Weakly mineralized	
ZF-1	1041.5	Platreef	PU3	Orthopyroxenite Pegmatoid	Pegmatoidal	Abundant Cr	Richly mineralized	LR1
ZF-1	1044.8	Platreef	PU3	Orthopyroxenite Pegmatoid	Pegmatoidal		Richly mineralized	LR1
ZF-1	1059.2	Platreef	PU1	Melanorite	Medium-grained		Richly mineralized	LR1
ZF-1	1075.2	Platreef	PU1	Norite	Medium-grained		Barren	
ZF-1	1085.8	Platreef	PU1	Melanorite	Medium-grained	Inch-scale layered	Weakly mineralized	
ZF-1	1095.7	Platreef	PU3	Orthopyroxenite Pegmatoid	Pegmatoidal	Abundant Cr	Richly mineralized	LR2
ZF-1	1096.8	Platreef	PU3	Orthopyroxenite Pegmatoid	Pegmatoidal	Cr Stringers	Richly mineralized	LR2
ZF-1	1097.2	Platreef	PU1	Feldspathic Orthopyroxenite	Medium-grained	Cr Stringers	Richly mineralized	LR2
ZF-1	1097.6	Platreef	PU1	Feldspathic Orthopyroxenite	Medium-grained	Abundant Cr	Richly mineralized	LR2
ZF-1	1111.2	Lower Critical	LCZ	Harzburgite	Medium-grained		Richly mineralized	LR3
ZF-1	1123.6	Lower Critical	LCZ	Harzburgite	Medium-grained		Weakly mineralized	
ZF-1	1138.2	Lower Critical	LCZ	Feldspathic Orthopyroxenite	Coarse-grained		Weakly mineralized	
MO-3	1330.7	Lower Main	LMZ	Norite	Medium-grained		Barren	
MO-3	1333.7	Platreef	PU1	Melanorite	Medium-grained		Weakly mineralized	
MO-3	1341.8	Platreef	PU1	Melanorite	Medium-grained		Weakly mineralized	
MO-3	1346.5	Platreef	PU1	Norite	Coarse-grained		Barren	

Table 2: Selected Trace Elements

Drill Hole	Depth m	V	Cr	Ni	Cu	Rb	Sr	Y	Zr	Nb
ZF-1	1001.5	145	915	441	55	3.2	162.8	6.01	12.85	0.53
ZF-1	1005.7	163	827	378	50	8.1	217.8	6.51	16.81	0.81
ZF-1	1010.2	172	894	438	57	5.0	177.6	7.16	10.42	0.30
ZF-1	1011.8	171	1,077	503	48	4.3	171.0	7.14	13.28	0.61
ZF-1	1012.8	138	924	427	56	8.1	217.4	6.91	19.75	0.98
ZF-1	1016.2	90	4,451	1,087	101	2.3	51.9	2.92	5.64	0.25
ZF-1	1019.3	103	4,496	1,361	208	5.7	46.6	3.82	6.52	0.28
ZF-1	1022.6	90	5,191	1,433	84	3.8	54.2	3.38	3.93	0.15
ZF-1	1025.1	76	6,486	2,429	28	5.6	37.0	3.33	2.95	0.13
ZF-1	1026.0	62	5,694	6,140	1,279	5.1	25.8	3.16	4.14	0.17
ZF-1	1027.8	148	1,963	2,553	897	5.9	104.8	5.12	5.33	0.18
ZF-1	1033.3	167	2,958	4,522	1,034	2.3	49.1	7.50	8.80	0.32
ZF-1	1039.6	138	3,827	1,074	58	3.6	100.5	7.30	14.20	0.38
ZF-1	1041.5	482	48,748	2,837	631	4.9	77.0	5.08	9.37	0.40
ZF-1	1044.8	142	3,717	1,153	106	3.4	44.6	7.77	12.57	0.54
ZF-1	1059.2	103	2,922	2,982	860	11.7	102.8	4.65	5.08	0.27
ZF-1	1075.2	114	1,821	612	20	19.9	178.1	3.54	5.54	0.17
ZF-1	1085.8	135	2,250	2,096	643	5.7	93.3	4.14	7.40	0.42
ZF-1	1095.7	715	125,597	3,053	585	11.7	68.3	2.53	10.52	1.11
ZF-1	1096.8	199	17,042	1,336	191	7.4	60.9	4.05	8.18	0.59
ZF-1	1097.2	198	19,886	2,705	766	11.2	91.3	3.34	9.85	0.64
ZF-1	1097.6	923	151,927	5,181	1,365	13.6	93.9	2.39	8.55	0.46
ZF-1	1111.2	104	21,783	3,112	19	9.3	9.1	2.32	6.80	0.42
ZF-1	1123.6	101	16,189	2,549	32	2.0	11.4	1.25	1.23	0.05
ZF-1	1138.2	85	2,530	6,470	900	5.4	43.7	2.11	1.95	0.08
MO-3	1330.7	93	1855	1511	371	6.4	93.7	3.32	6.93	0.38
MO-3	1333.7	83	1875	859	95	5.4	84.3	2.45	4.47	0.26
MO-3	1341.8	113	2968	1604	279	5.9	89.7	2.59	3.81	0.35
MO-3	1346.5	76	1302	908	112	19.4	167.5	2.59	6.95	0.34

Table 3: Radiogenic Isotope Data

Drill Hole	Depth m	Rb ppm	Sr pm	$^{87}Rb/^{86}Sr$	$^{87}Sr/^{86}Sr$	2SD	$^{87}Sr/^{86}Sr0$ 2.055 Ga	Sm ppm	Nd ppm	$^{147}Sm/^{144}Nd$	$^{143}Nd/^{144}Nd$
ZF-1	1001.5	3.2	162.8	0.0547	0.71045	0.0000047	0.70883	0.8181	3.5911	0.1372	0.51153
ZF-1	1005.7	8.1	217.8	0.1049	0.71243	0.0000070	0.70932	0.9761	4.4232	0.1329	0.51143
ZF-1	1010.2	5.0	177.6	0.0797	0.71119	0.0000092	0.70883	0.9722	3.8822	0.1509	0.51167
ZF-1*	1011.8	4.3	171.0	0.0715	0.71076	0.0000090	0.70865	0.9519	3.9947	0.1436	0.51148
ZF-1	1012.8	8.1	217.4	0.1056	0.71211	0.0000061	0.70899	0.9047	4.3052	0.1266	0.51141
ZF-1*	1016.2	2.3	51.9	0.1238	0.71560	0.0000050	0.71193	0.2601	1.1148	0.1406	0.51158
ZF-1	1019.3	5.7	46.6	0.3439	0.71865	0.0000053	0.70846	0.3433	1.4163	0.1460	0.51165
ZF-1	1022.6	3.8	52.6	0.2033	0.71687	0.0000057	0.71085	0.2132	0.7647	0.1679	0.51161
ZF-1	1025.1	5.6	37.0	0.4300	0.72427	*0.0000073*	0.71154	0.2611	0.9762	0.1611	0.51146
ZF-1	1026.0	5.1	25.8	0.5566	0.72747	0.0000074	0.71099	0.2932	1.1570	0.1527	0.51164
ZF-1	1027.8	5.9	112.4	0.1484	0.71336	0.0000070	0.70897	0.5804	2.2971	0.1522	0.51171
ZF-1	1033.3	2.3	49.1	0.1312	0.71272	0.0000076	0.70884	0.8778	3.3469	0.1580	0.51162
ZF-1	1039.6	3.6	100.5	0.1006	0.71398	0.0000066	0.71100	0.7939	3.3504	0.1427	0.51157
ZF-1	1041.5	4.9	77.0	0.1814	0.71556	0.0000072	0.71019	0.5965	2.4666	0.1457	0.51155
ZF-1	1044.8	3.4	44.6	0.2142	0.71575	0.0000085	0.70940	0.8839	3.6541	0.1457	0.51165
ZF-1	1059.2	11.7	102.8	0.3218	0.72105	0.0000066	0.71152	0.5407	2.4035	0.1355	0.51152
ZF-1	1075.2	19.9	178.1	0.3160	0.71833	0.0000078	0.70898	0.4627	2.0409	0.1366	0.51148
ZF-1	1085.8	5.7	93.3	0.1722	0.71489	0.0000048	0.70979	0.4812	2.0152	0.1438	0.51154
ZF-1	1095.7	11.7	68.3	0.4834	0.72352	0.0000075	0.70921	0.4056	2.1557	0.1133	0.51115
ZF-1	1096.8	7.4	60.9	0.3422	0.71928	0.0000068	0.70915	0.4737	2.0702	0.1379	0.51155
ZF-1	1097.2	11.2	91.3	0.3478	0.71993	0.0000065	0.70963	0.3921	1.7710	0.1334	0.51141
ZF-1	1097.6	13.6	93.9	0.4088	0.72115	0.0000124	0.70904	0.3246	1.4557	0.1343	0.51186
ZF-1	1111.2	9.3	9.1	2.8768	0.78928	0.0000076	0.70410	0.3928	1.8236	0.1298	0.51134
ZF-1	1123.6	2.0	11.4	0.4993	0.72059	0.0000054	0.70581	0.1449	0.5070	0.1721	0.51193
ZF-1	1138.2	5.4	43.7	0.3466	0.72260	0.0000069	0.71233	0.1578	0.5288	0.1798	0.51212
MO-3	1330.7	6.4	93.7	0.1933	0.71455	0.0000066	0.70883	0.3527	1.5797	0.1345	0.51150
MO-3	1333.7	5.4	84.3	0.1799	nd	nd	nd	0.2749	1.3164	0.1258	0.51138
MO-3	1341.8	5.9	89.7	0.1853	0.71717	0.0000062	0.71168	0.2353	1.0187	0.1391	0.51148
MO-3	1346.5	19.4	167.5	0.3266	0.72188	0.0000063	0.71221	0.2477	1.1444	0.1304	0.51143

*Duplicate Sm and Nd

2SD	$^{143}Nd/^{144}Nd0$ 2.055 Ga	ε_{Nd}
0.0000057	0.50967	-5.97
0.0000055	0.50963	-6.83
0.0000052	0.50963	-6.80
0.0000042	0.50964	-8.53
0.0000035	0.50969	-5.55
0.0000081	0.50968	-5.80
0.0000100	0.50967	-5.91
0.0000065	0.50934	-12.48
0.0000049	0.50928	-13.73
0.0000059	0.50958	-7.84
0.0000047	0.50965	-6.49
0.0000054	0.50948	-9.74
0.0000051	0.50964	-6.61
0.0000056	0.50958	-7.86
0.0000049	0.50968	-5.85
0.0000048	0.50969	-5.60
0.0000057	0.50963	-6.81
0.0000055	0.50959	-7.60
0.0000044	0.50962	-7.08
0.0000055	0.50969	-5.67
0.0000058	0.50961	-7.20
0.0000062	0.51004	1.21
0.0000052	0.50959	-7.60
0.0000083	0.50960	-7.36
0.0000060	0.50969	-5.60
0.0000055	0.50968	-5.81
0.0000055	0.50968	-5.82
0.0000049	0.50960	-7.36
0.0000062	0.50967	-6.08

Table 4: Summary of Isotopic Data (averages) for Akanani and Up-dip Areas

Zone or Subzone	Area	$^{87}Sr/^{86}Sr0$ Number	$^{87}Sr/^{86}Sr0$ Avg	$^{87}Sr/^{86}Sr0$ S.D.	ε_{Nd} Number	ε_{Nd} Avg	ε_{Nd} S.D.	Age Ga
LMZ	Akanani (ZF-1)	5	0.70892	0.00025	5	-6.73	1.14	2.055
LMZ	Akanani (MO-3)	1	0.70883	-	1	-5.81	-	2.055
LMZ	Overysel[1]	1	0.70790	-	1	-	-	2.050
LMZ	Overysel[2]	6	0.71344	0.00869	5	-7.84	0.65	2.060
LMZ	Sandsloot[3]	1	0.71037	-		-	-	2.060
PU	Akanani (ZF-1)	14	0.70972	0.00106	13	-6.75	1.21	2.055
MMR	Akanani (ZF-1)	3	0.71113	0.00037	3	-11.35	3.11	2.055
PU	Akanani (MO-3)	2	0.71194	0.00037	3	-6.42	0.83	2.055
PU	Overysel[1]	6	0.71598	0.00443				2.050
PU	Sandsloot[3]	2	0.71309	0.00086	2	-7.15	0.26	2.060
LCZ	Akanani	3	0.70741	0.00435	3	-6.85	1.09	2.055

[1]Data of Cawthorn et al. (1985);[2]Data of Pronost et al. (2008);[3]Data of Harris & Chaumba (2001)

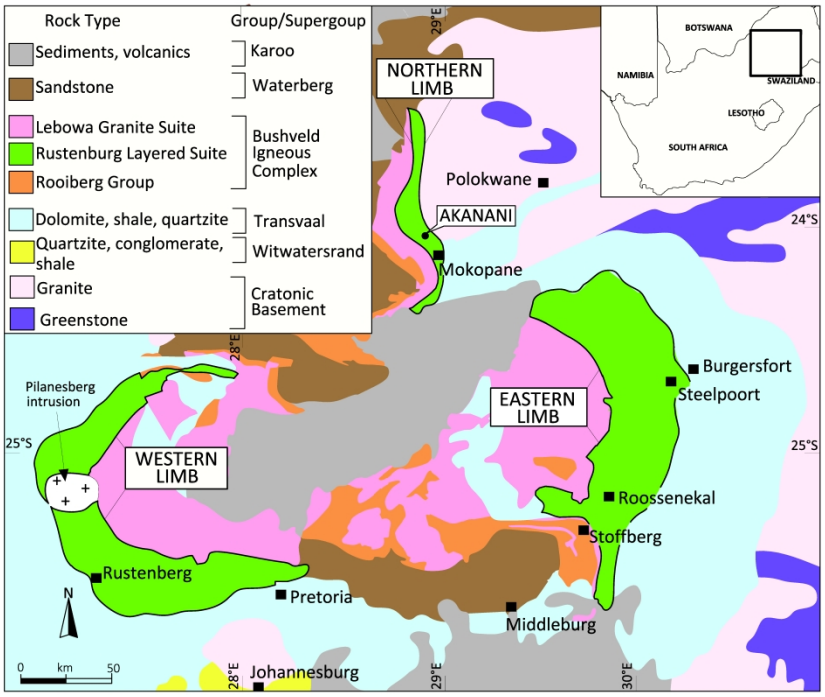

Fig. 1. Regional map of the Bushveld Igneous Complex showing location of Akanani in the Northern Limb. The Rustenburg Layered Suite has cut down through the metasediments of the Transvaal Supergoup into granite of the cratonic basement. The older felsites of the Rooiberg Group and younger granite-granophyre of the Lebowa Granite Suite primarily occur in the centre of the Transvaal basin. Simplified from the 1:1,000,000 scale map published by the Council for Geoscience.

297x210mm (600 x 600 DPI)

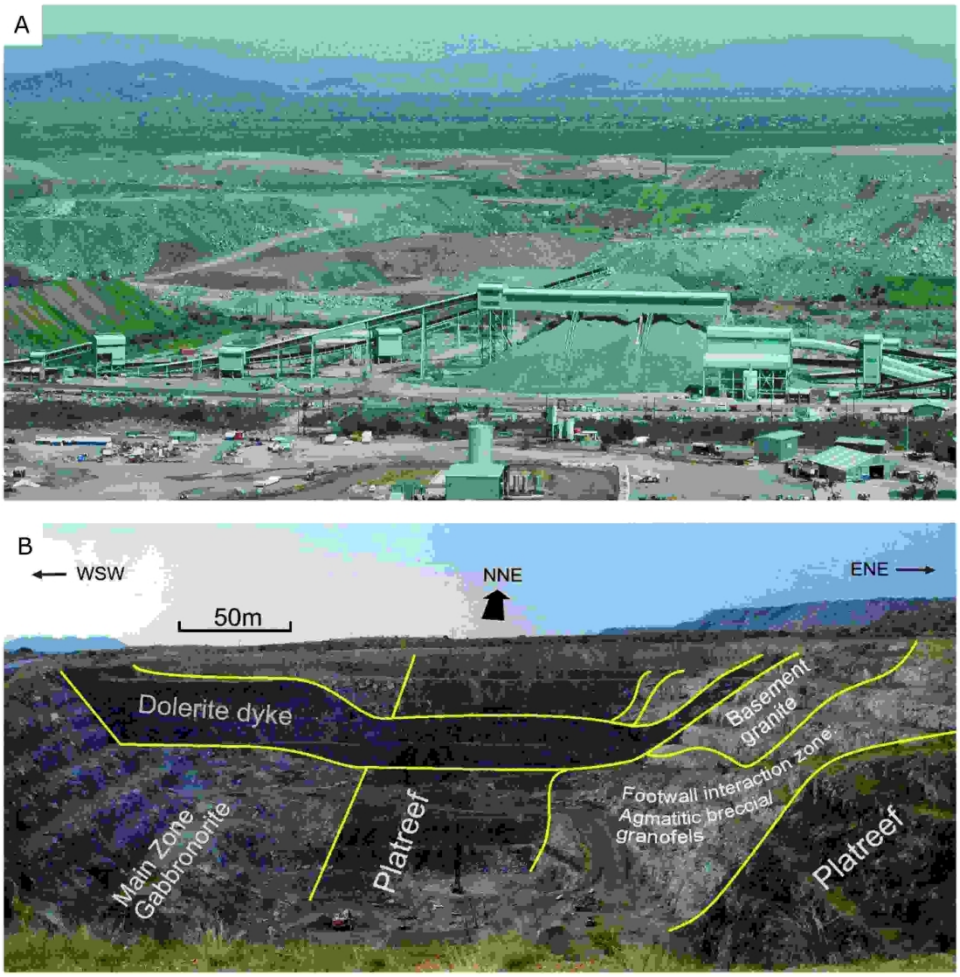

209x212mm (300 x 300 DPI)

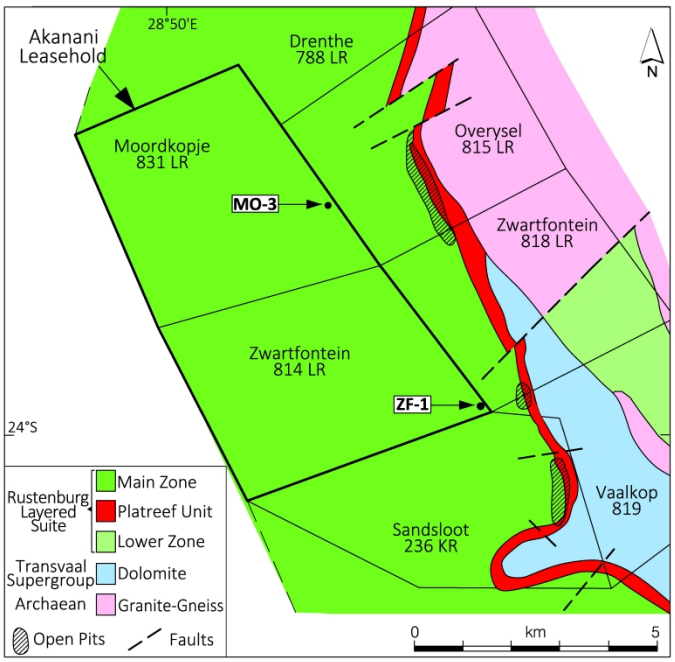

Fig. 3. Simplified geological map showing location of Akanani Leasehold (Zwartfontein 814 LR and Moordkopje) and location of drill-holes studied here. Also shown are the open pit mines on up-dip properties of Sandsloot, Vaalkop, Zwartfontein 818LR, and Overysel. The Rustenburg Layered Suite rests on dolomite of the Transvaal Supergroup in the southern part of the area and on Archaean granite-gneiss in the northern part. Simplified from the 1:250,000 scale maps (2328 and 2428) published by the Council for Geoscience.

297x210mm (600 x 600 DPI)

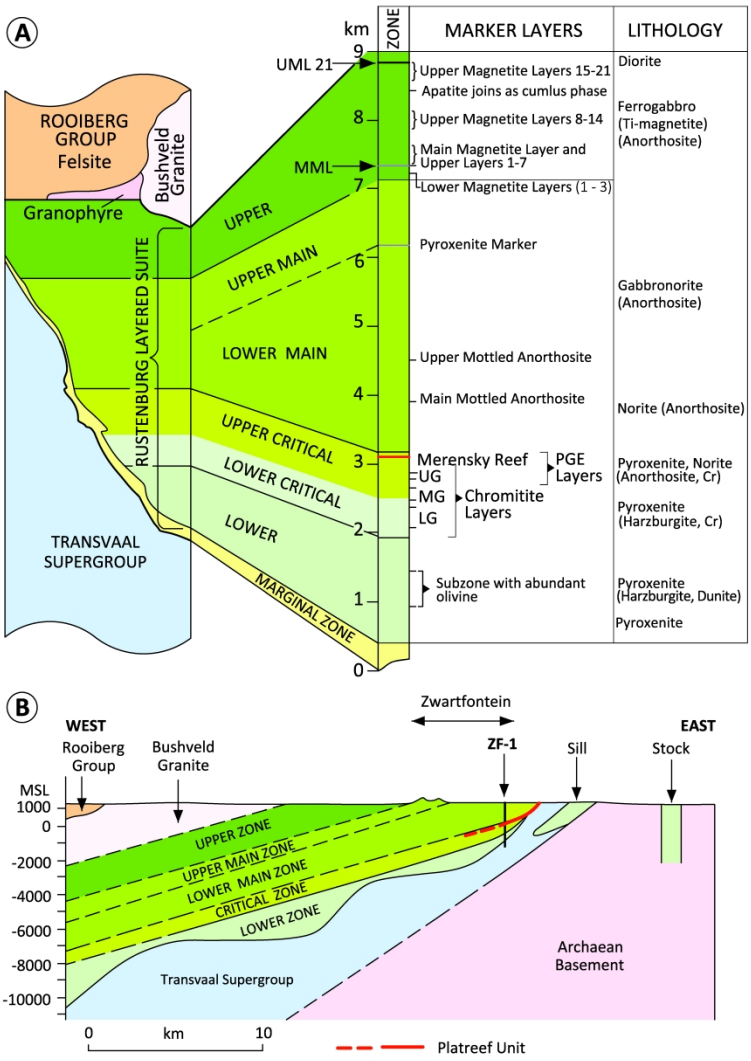

Fig. 4. (a) Generalized stratigraphic column for the Eastern Limb of the Bushveld Igneous Complex showing subdivision of the Rustenburg Layered Suite into zones; (b) Schematic section of the Northern Limb at Akanani aligned with drill-hole ZF-1, Zwartfontein 814 LR. Interpretation based on the 1:250,000 scale map 2328 published by the Council for Geoscience and drilling at Akanani and based on correlation of the Platreef Unit with the UCZ.

210x297mm (600 x 600 DPI)

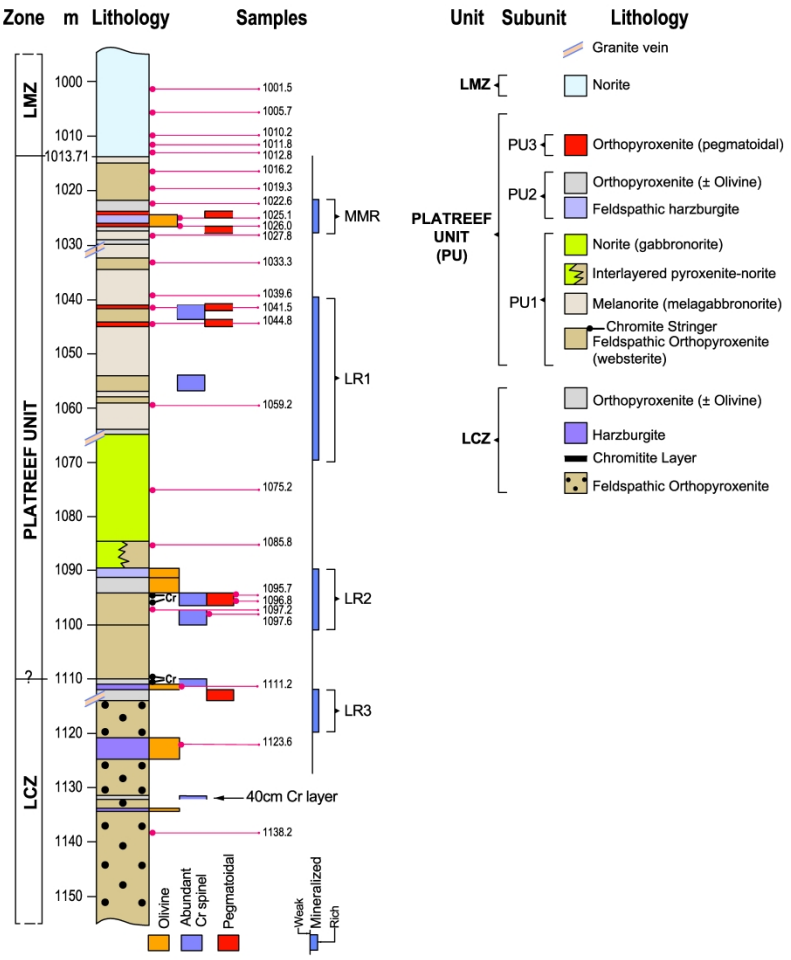

Fig. 5. Stratigraphic log for drill-hole ZF-1 showing basal part of the Lower Main Zone (LMZ), Platreef Unit, and upper part of the Lower Critical Zone (LCZ). Sample positions annotated relative to depth. Occurrence of olivine, Cr-spinel, and lithologies with a pegmatoidal texture highlighted. Lithologies simplified in parts of column due to scale constraints. The proportion of orthopyroxene and clinopyroxene is variable and the subordinate presence of clinopyroxene-rich lithologies is denoted by brackets. Grouping of lithologies into the PU1, PU2 and PU3 subunits is interpretative. Identification of the Main Mineralized Reef (MMR) and Lower Reefs (LR1-3) is for descriptive purposes and has no bearing on potentially mineable orebodies.

210x297mm (600 x 600 DPI)

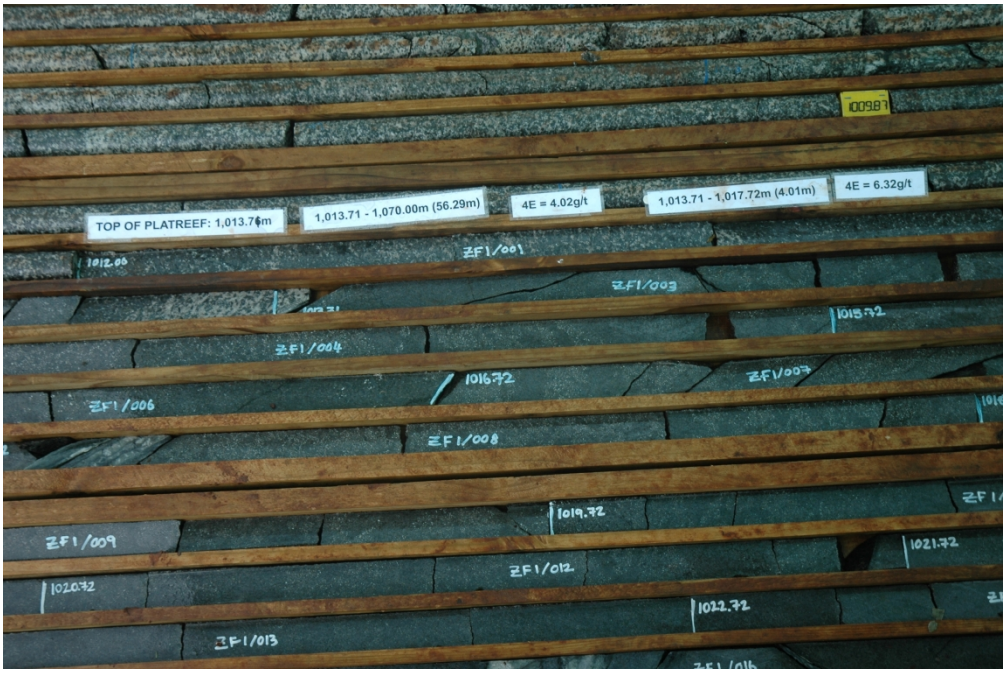

Fig. 6. The contact between norite of the Lower Main Zone and the distinctly more mafic Platreef Unit occurs at a depth of 1013.71 m in drill-hole ZF-1. Average grades of 4.02 g/t over a width of 56.29 m, and 6.32 g/t over a width of 4.01 m, are for 3PGE+Au using base of the Lower Main Zone as datum selected by the mining company.

254x169mm (300 x 300 DPI)

209x170mm (300 x 300 DPI)

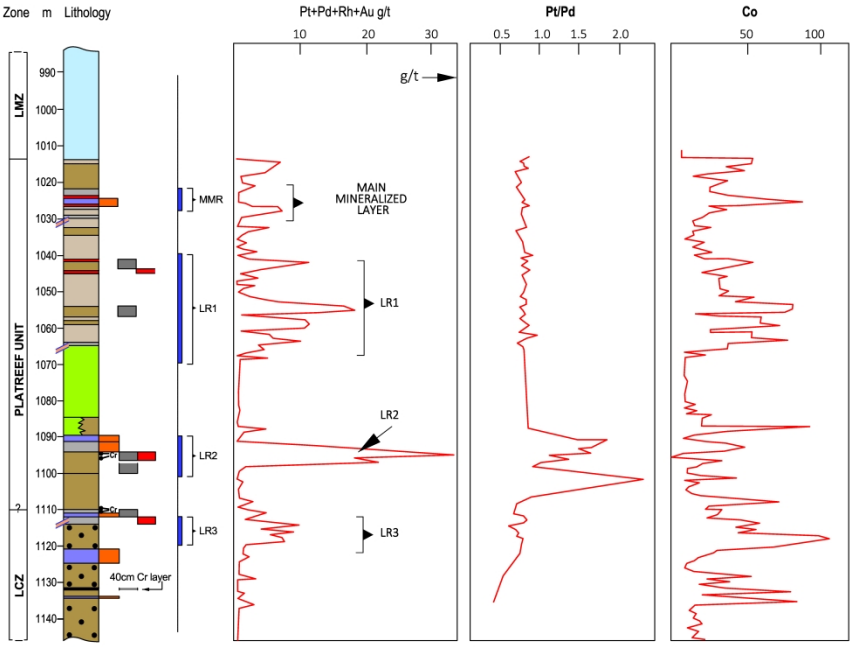

Fig. 8. The vertical distribution of Pt, Pd, Rh, and Au, the Pt/Pd ratio, and the whole-rock Co content in drill-hole ZF-1 define four mineralized "reefs". Data based on commercial assays provided by the mining company.

297x210mm (600 x 600 DPI)

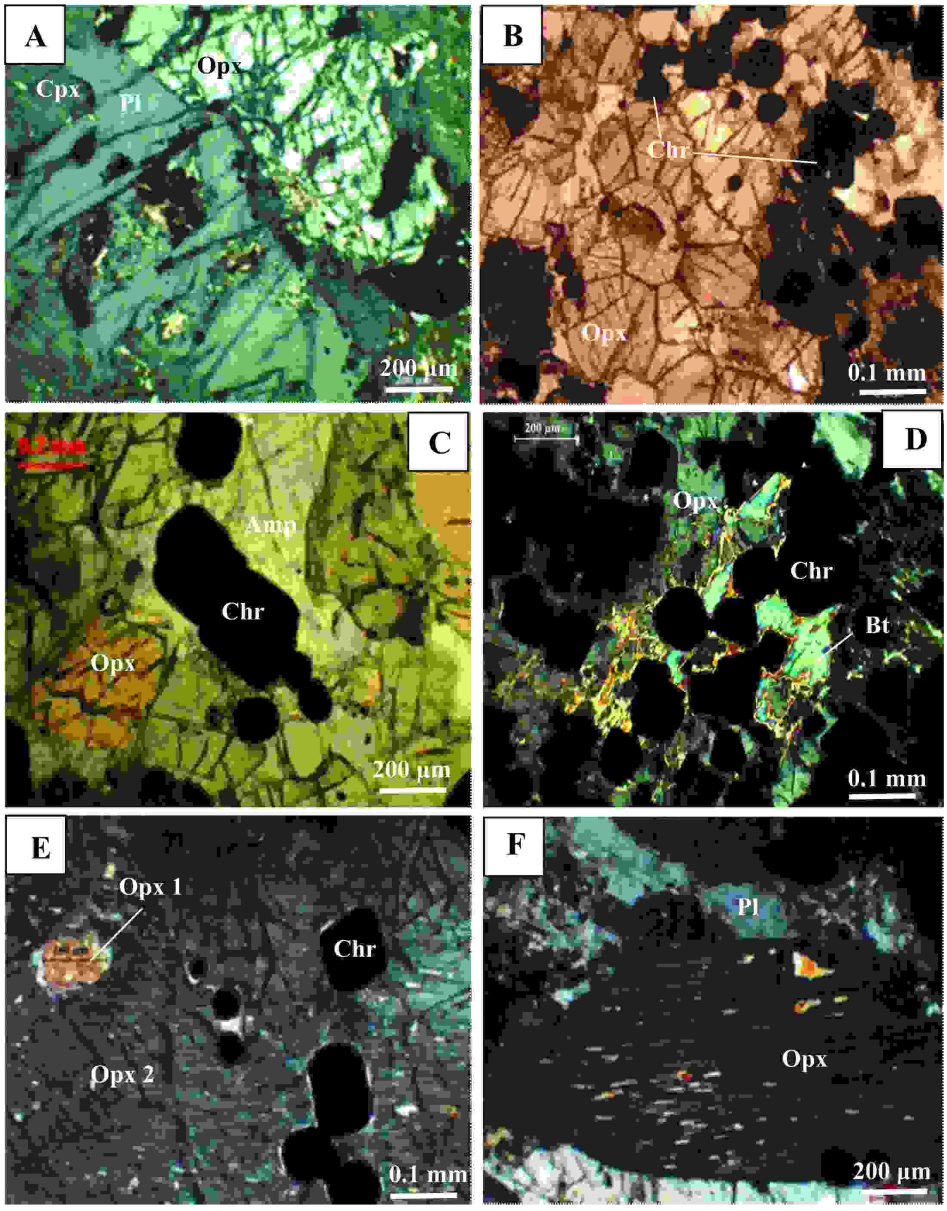

185x236mm (300 x 300 DPI)

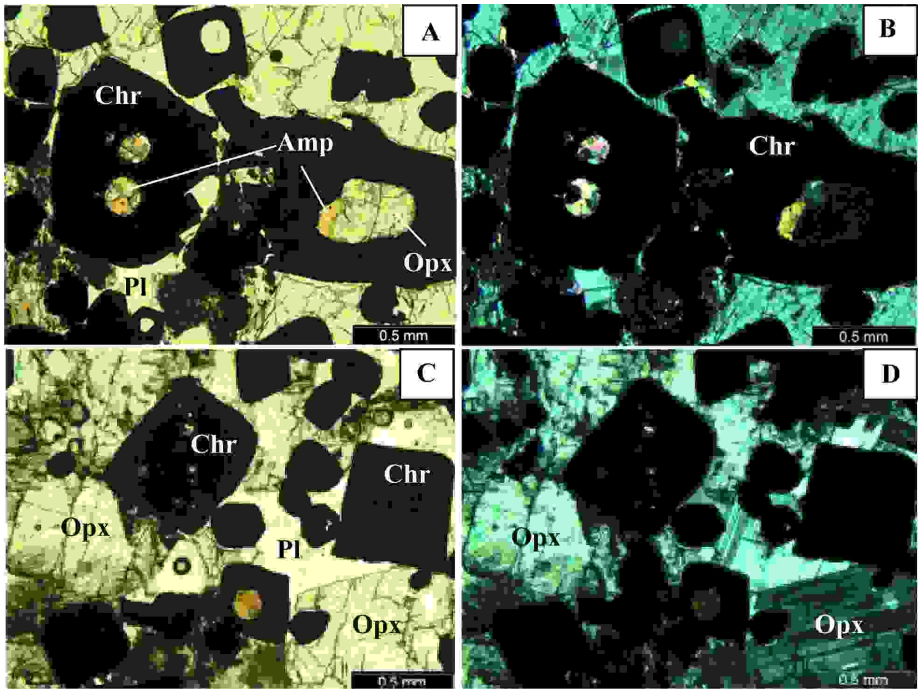

181x124mm (300 x 300 DPI)

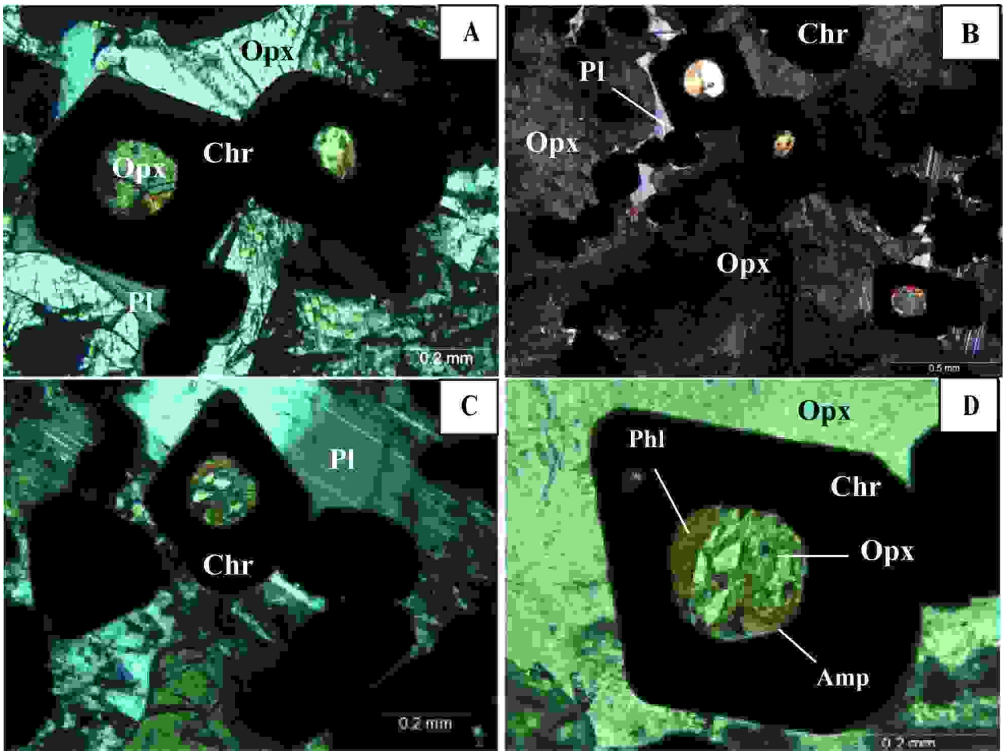

166x124mm (300 x 300 DPI)

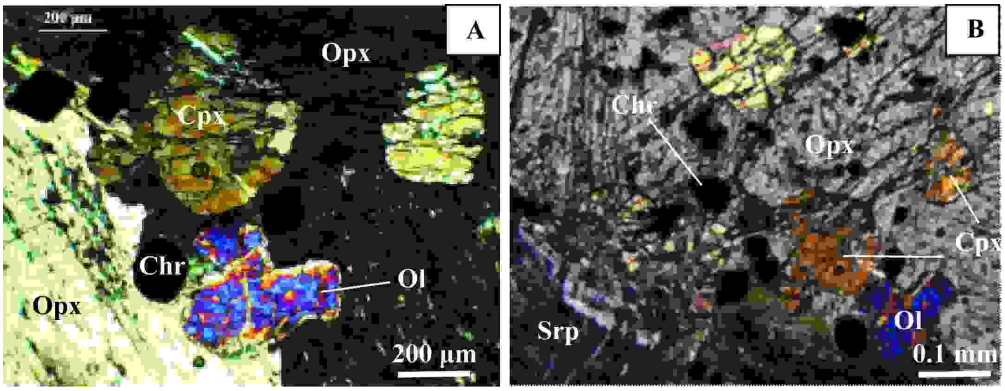

181x69mm (300 x 300 DPI)

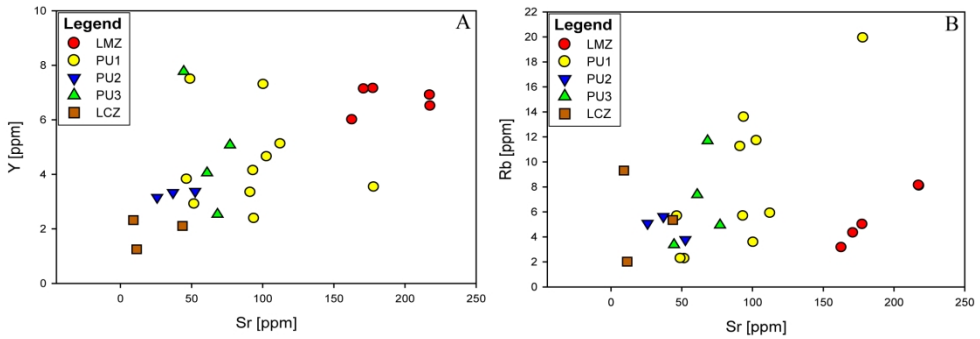

Fig. 13. Plot of Sr against Y and Rb based on whole-rock compositions for samples from drill-hole ZF-1.

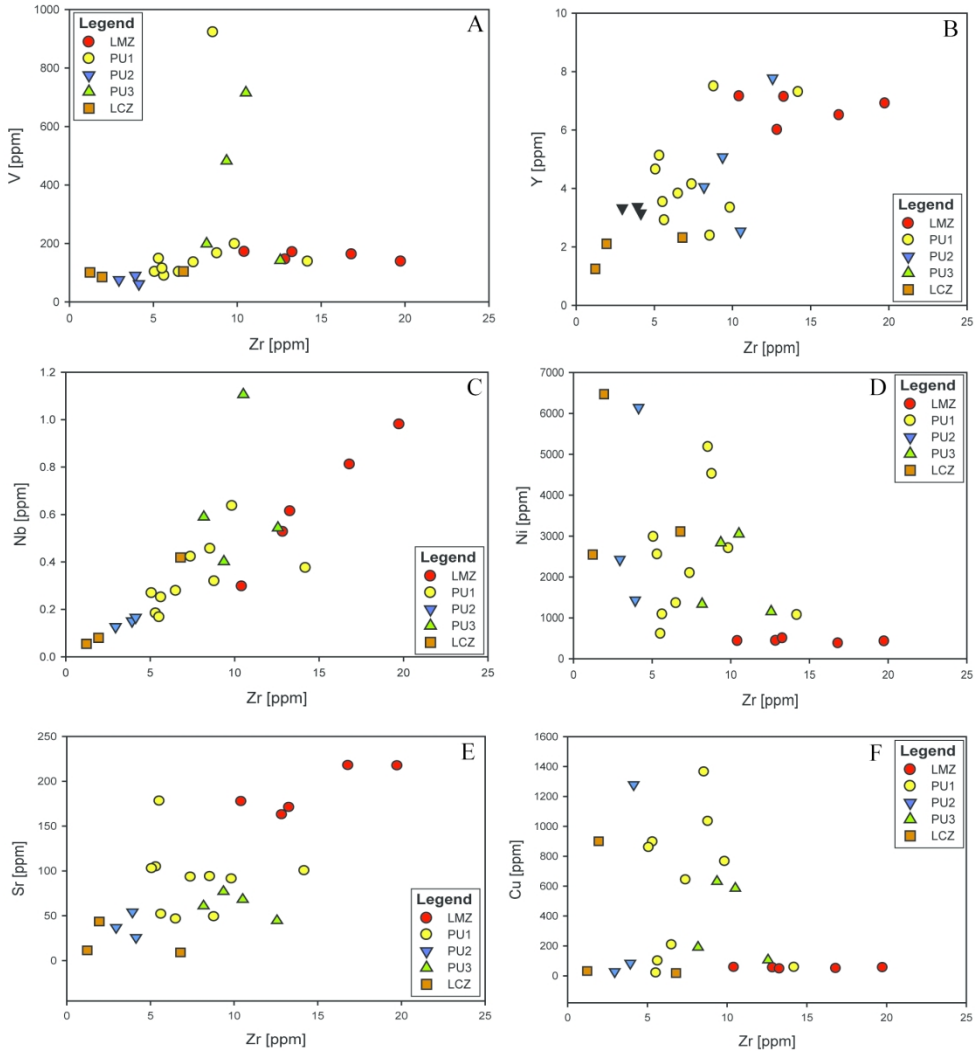

Fig. 14. Selected trace elements plotted against Zr based on whole-rock compositions for samples from drill-hole ZF-1.

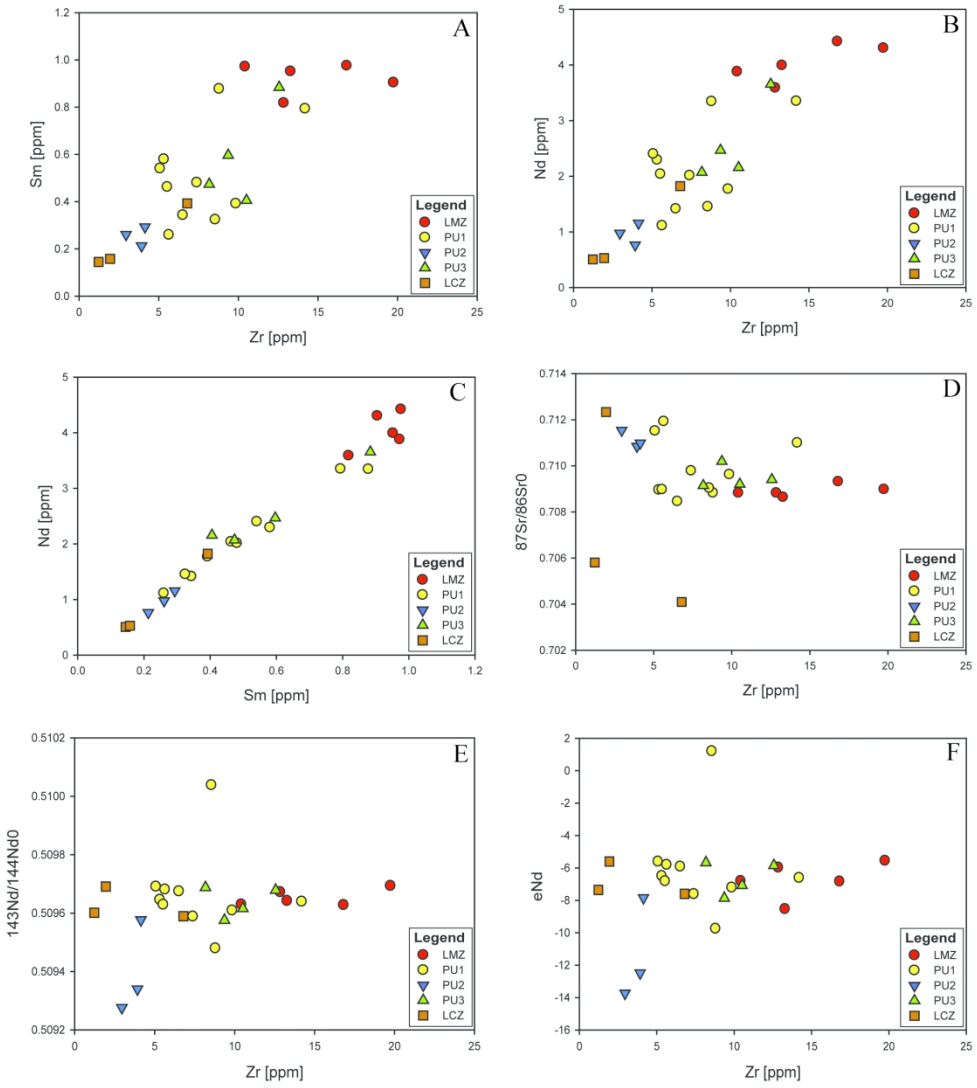

Fig. 15. Selected trace elements plotted against Zr based on whole-rock compositions for samples from drill-hole ZF-1.

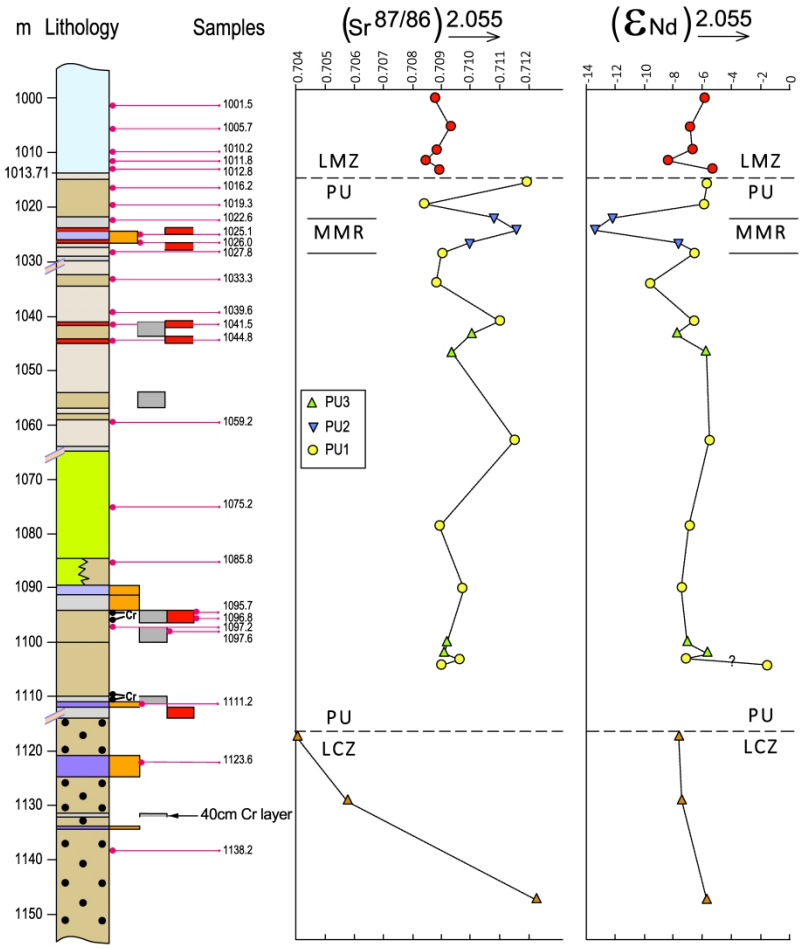

Fig. 16. Plot of the Sr-initial ratio and the □Nd value against height for samples from drill-hole ZF-1.

210x297mm (600 x 600 DPI)

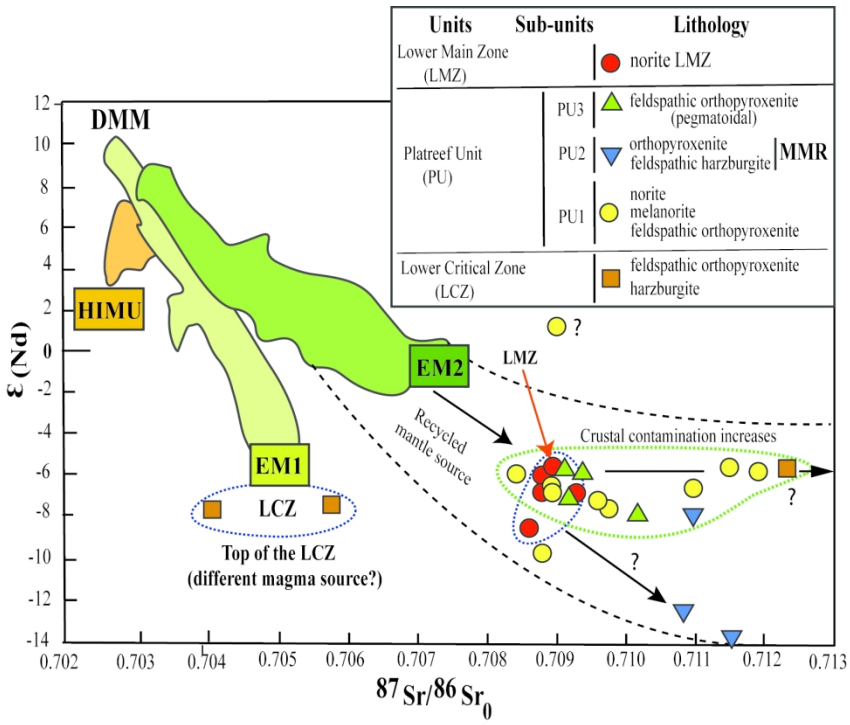

Fig. 17. Plot of the Sr-initial ratio against the □Nd value for samples from drill-hole ZF-1. Fields labelled DMM (Depleted Mantle), HIMU, EM1 (Enriched Mantle 1) and EM2 (Enriched Mantle 2) after Zindler & Hart (1986). The general trend suggests an extremely enriched mantle source, characteristic for old, recycled lithospheric mantle.